

Practical magnetotellurics in a continental rift environment

G.R. Jiracek, V. Haak, and K.H. Olsen

Jiracek, G.R., Haak, V., and Olsen, K.H., 1995, Practical magnetotellurics in a continental rift environment; *in* K.H. Olsen, ed., Continental rifts: evolution, structure and tectonics: New York, Elsevier, 103-129.

3E.1. Introduction

It is no exaggeration to say that surface measurements of deep electrical resistivity may hold the key to understanding how continental rifts develop. This is so because low resistivities detected in the mid-to-lower crust in rift zones reflect conditions that control the strain rate, and therefore, the style and extent of tectonic deformation. Although low resistivities in active continental rifts probably are associated with fluids (either water and/or magma), it is their origin, their accumulation, and their influence that are critical. For example, is the strength of the lithosphere (and its brittle-ductile profile with depth) dominantly controlled by accumulations of high pressure H_2O-CO_2 pore fluids, and, if so, what are the origins of these fluids? By better defining the depth and lateral extent of conductive occurrences in the crust and by carefully contrasting them with other geophysical measurements, important constraints on deep physical conditions will follow. Attempts at such syntheses are not new, e.g., Garland (1975), Hermance (1982), Haak and Hatton (1986), and Keller (1989) have made this effort, but it is clear that many new correlations are very important (e.g., Jodicke, 1992; Jones, 1992; Hyndman et al., 1993; Jiracek, 1995) and others will be forthcoming as research continues.

In this contribution we provide a self-contained but brief overview of the principal technique used to derive the deep subsurface distribution of electrical resistivity—namely the magnetotelluric (MT)

method. MT exploration of the Earth has evolved to the status of a mature science during the past two decades with the advent of digital instrumentation, real-time processing, and sophisticated, robust analysis techniques showing increasing promise for interpreting complex, three-dimensional (3-D) electrical structures in the Earth. MT and other geoelectromagnetic methods are probably the least understood of geophysical techniques. This results in the humorous expectation among MT practitioners of the “MT (empty) stare”, a look on colleagues’ faces when the conversation turns to MT results.

Magnetotellurics is the recording and study of naturally occurring electric and magnetic fields at the Earth’s surface. The object of MT is to map the electrical properties of the Earth from the surface to many tens of km and to relate these geoelectric properties to the physical state and the tectonic processes that deform the Earth. There are many everyday examples of electromagnetic (EM) radiation such as radio waves, microwaves, and visible light itself (Fig. 3E-1). These common phenomena are at frequencies much higher than those used in most MT applications and, except for celestial light sources, the examples above are of man-made origin. There are several electromagnetic geophysical techniques that use transmitted energy from man-made sources (so-called *active sources*). Indeed, there are forms of MT that use controlled sources; however, to probe deep into the Earth, much more powerful energy sources at low frequencies are required. The sun is the major *passive source* for this application. A dis-

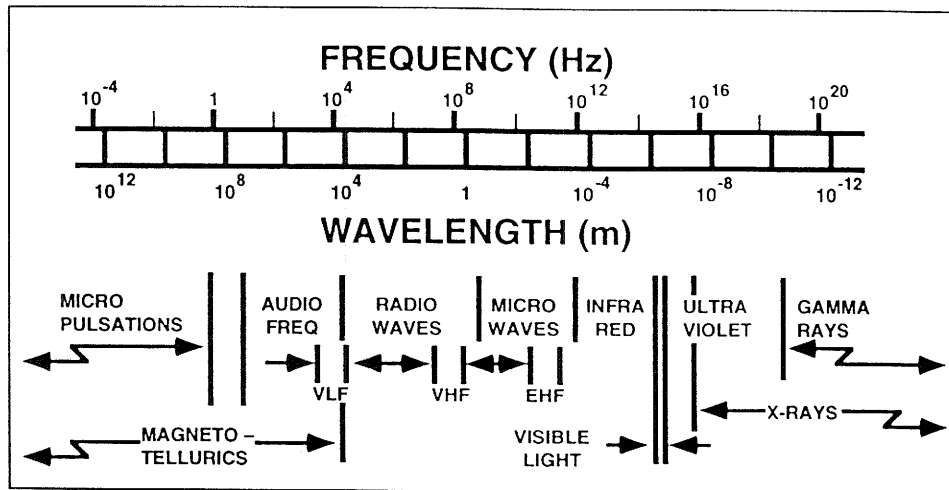


Fig. 3E-1. Twenty-four decades of the electromagnetic spectrum. Abbreviations, VLF, VHF, and EHF designate very low frequency, very high frequency, and extremely high frequency bands, respectively. The magnetotelluric frequency range extends from about 10^{-4} to 10^{14} Hz.

advantage of a passive source is that it cannot be controlled by the experimenter. For example, MT measurements must depend on the uncertain energy levels in solar emissions.

When EM fields from any source encounter an obstacle such as the Earth, some energy penetrates (transmits) and some reflects. The reflected waves constructively and destructively interfere with the incident waves, and the transmitted waves are attenuated before they reflect from subsurface discontinuities. The Earth is a much better electrical conductor than air so the total electric field measured at the surface by MT is nearly zero because there is near cancellation of the incident field by the reflected field. The magnitude of the reflected electric field is a very large proportion (nearly 100%) of the incident field. The consequence is that the transmitted electric field is only a tiny fraction of the incident field. Fortunately this fraction is not zero, otherwise there would be no MT method. As it is, the wave propagation mechanism changes at the Earth's surface from that which dominates in an insulator (the air) to that which dominates in a conductor (the Earth). The technical description of this

change embraces the end member processes of EM propagation, namely displacement currents and conduction currents, respectively. This chapter discusses the physics of these consequences and how they are used in practice to apply the MT method. In the first sections below, we try to provide a non-specialist geoscientist with a working knowledge of the MT method and its terminology. Then, these basic MT principles are applied both to synthetic and to actual continental rift data in order to illustrate the value and limitations of the method. Finally, we address the ultimate question of what derived resistivity values may mean through a discussion of possible connections between the geoelectric results and the rheology of continental rifts. The focus will be on findings from the lithosphere (mainly the crust) where excellent data have been accumulated during the last 15 years. Results from deeper—in the asthenosphere—are equally important, and historically were the first to be reported. However, most recent MT studies have targeted the crust where correlations with other geophysical data have been particularly rewarding.

3E.2. Magnetotelluric measurements

The MT method is a relatively new geophysical technique. The first paper on MT was written less than 50 years ago by the distinguished Soviet academician, A.N. Tikhonov (1950). Even so, the fundamentals of the method are a direct consequence of the classical electromagnetic (EM) theory established more than 100 years ago by the work of Ampere, Faraday, and Maxwell. Tikhonov's (1950) seminal contribution was to show that, at low frequencies, the spatial derivative of the horizontal component of the Earth's magnetic field (\mathbf{H}) is proportional to the orthogonal component of the electric field (\mathbf{E}) [vector quantities are shown in **bold-face**]. He used previously published diurnal \mathbf{H} data from magnetic observatories at Tucson, Arizona, USA, and from Zui, USSR, to estimate the thickness and electrical conductivity of the crust at these sites. The first western paper on MT was published by Cagniard (1953) in which he developed the formulas relating \mathbf{E} and \mathbf{H} on the surface of a layered medium with an incident plane wave. The works of Tikhonov and Cagniard form the basis of one-dimensional (1-D) MT analysis and this is often referred to as the *Tikhonov-Cagniard model*.

The practicality of the Tikhonov-Cagniard model of MT was soon challenged by Wait (1954), who argued that the proportionality between orthogonal \mathbf{E} and \mathbf{H} fields at the Earth's surface was valid only if the source fields do not vary appreciably over a characteristic distance called the *skin depth* (skin depth will be rigorously defined later). Madden and Nelson (1964) came to the defense of the Tikhonov-Cagniard model by showing that when the source's horizontal wavelength is much greater than the skin depth, as it is for the Earth, the model remains valid. Later, Dmitriev and Berdichevsky (1979) further proved that the horizontal magnetic field components need not be uniform, but can vary linearly over a layered earth.

Magnetotelluric source fields can be classified as originating either from lightning or from solar activity. Roughly speaking, fields below a frequency of 1 Hz are caused by the Sun; above 1 Hz, fields are due to worldwide thunderstorm activity. Fields due to solar activity result from complex interac-

tions between the solar wind (charged particles ejected from the Sun) and the Earth's magnetosphere. In particular, the continuous and irregular pulsations of the solar wind change the shape and size of the magnetosphere and cause it to vibrate like an extra-terrestrial jello. The resulting complex hydromagnetic waves are a major source of MT energy in a broad frequency band between 1 and about 10^{-4} Hz (Fig. 3E-1). Energy in hydromagnetic waves is transformed into propagating electromagnetic waves after passing through the electrically conductive, anisotropic ionosphere. This interaction forms large horizontal sheets of current in the ionosphere. Indeed, current systems of the daily variation are literally of hemispherical proportions.

Electromagnetic energy from lightning discharges around the world propagates in an atmospheric waveguide formed by the Earth and the ionosphere. This waveguide has resonance frequencies where energy is enhanced; e.g., the first Schumann resonance at 7.8 Hz has a wavelength equal to the circumference of the Earth. At frequencies of about 2 kHz, the waveguide is absorbing and energy in the natural electromagnetic spectrum is very low.

The physics of the interactions of the solar wind with the Earth's magnetosphere/ionosphere and the propagation of energy from distant lightning discharges is the subject of considerable research. Clear introductory discussions appear in Rokityansky (1982) and Vozoff (1991). From the standpoint of applying the MT method, there must be sufficient energy in the MT frequency band (Fig. 3E-1) and the incident plane wave assumption of the Tikhonov-Cagniard model must be valid. The latter is a fundamental assumption in applying the MT method; its validity depends on the location, size, and complexity of the source fields and their distances from the observation site. For example, a location at high magnetic latitudes (auroral latitudes) on the Earth's surface would be inappropriate during times of intense magnetic storms, but a mid-latitude site might be acceptable at the same time. Measurements taken during nearby thunderstorm activity would not meet the plane wave criterion, whereas waves from distant lightning can be properly treated as incident plane waves.

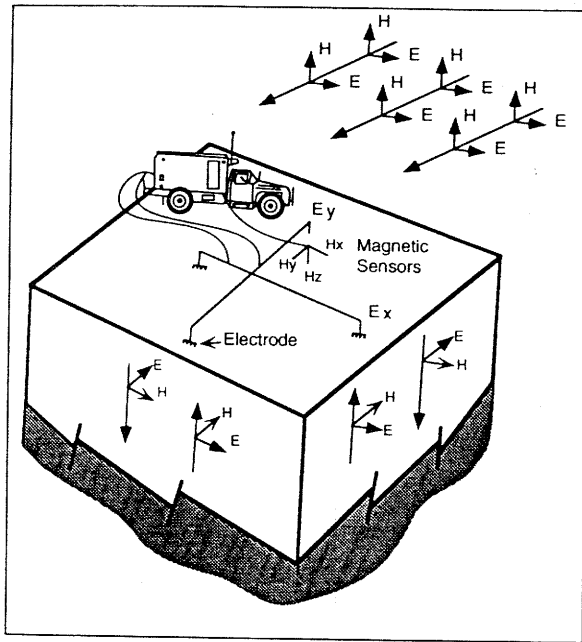


Fig. 3E-2. Magnetotelluric field layout with schematic incident, reflected, and transmitted propagating electromagnetic fields (redrawn from Sternberg et al., 1984).

The \mathbf{E} and \mathbf{H} fields measured at the surface of the Earth are samples of a stochastic (random) process since the solar wind and lightning activity are random variables of time and space. Therefore, the collection of all possible field measurements is unknown and infinite since we have no exact spatial-temporal knowledge of the underlying processes. Thus, at first it appears that the best one could hope for with such measurements would be statistical estimates of desired quantities. For example, only statistical probabilities can be used to describe the finite, known samples in the process of throwing a single die with six faces. If such were the case with MT measurements, the method would be of very limited value. What is needed to derive deterministic quantities is a measure—or measures—that when recorded now are the same as they were in the past or as they will be in the future. Clearly, the \mathbf{E} and \mathbf{H} fields themselves do not satisfy this property which is called *statistical stationarity*. Fortunately, there are such quantities in the MT case; they are the spectral ratios of the \mathbf{E} to \mathbf{H} field components. The “trick”

therefore, that enables practical use of the MT method is to take time measurements of \mathbf{E} and \mathbf{H} , convert them into their frequency representations, and then compute the \mathbf{E}/\mathbf{H} ratios. The conversion from time to frequency domain measurements is usually done by Fourier transforming via a computer algorithm such as the Fast Fourier Transform (FFT).

Physical measurements of the \mathbf{E} and \mathbf{H} fields are commonly made as shown schematically in Figure 3E-2. Orthogonal, horizontal \mathbf{E} fields are recorded by measuring the time-varying potential differences (voltages) between two nonpolarizing electrodes at the surface of the Earth. The ratio of these voltages divided by the horizontal distances (typically a few 100 m) are approximations of the E_x and E_y time-varying fields. Three perpendicular components of magnetic fields are normally obtained using induction coils which yield the time derivatives of the magnetic x , y , and z fields. Upon integration, one obtains the required H_x , H_y , and H_z time-varying fields. Magnetic fields can be measured directly by SQUID (Superconducting Quantum Interference Device) magnetometers, as was common in the late 1970s and early 1980s, but more recently, the development of highly sensitive, low noise induction coils has largely replaced SQUID measurements.

3E.3. Basic magnetotelluric principles

Simple manipulation of Maxwell's equations (Faraday's and Ampere's laws) together with the constitutive relations for a homogeneous linear isotropic medium yields the general electromagnetic (EM) *wave equation* for the time-varying vector \mathbf{E} field in charge-free regions (e.g., Ward and Hohmann, 1988),

$$\nabla^2 \mathbf{E} = \mu \left(\sigma \frac{\partial \mathbf{E}}{\partial t} + \epsilon \frac{\partial^2 \mathbf{E}}{\partial t^2} \right). \quad (1)$$

Here, μ is the magnetic permeability (in henrys/m, H/m), σ is the electric conductivity (in siemens/m, S/m), and ϵ is the electric permittivity (in farads/m, F/m); these are the physical quantities that describe the EM properties of a material. In most geophysical EM applications, μ can be assumed to have its free space value, μ_0 , and, as we shall soon see, the permittivity term in Eq. 1 can be neglected. This

places the ultimate emphasis on the conductivity as the principal diagnostic electrical parameter for the Earth. For purely traditional reasons geophysicists usually report the reciprocal of the conductivity which is the resistivity, ρ . Resistivity units are ohm-meters (ohm-m) since the siemen and the ohm are reciprocal units. Because, for practical reasons mentioned earlier, we want the \mathbf{E} and \mathbf{H} values as functions of frequency, it is convenient to immediately write the equivalent of the wave equation in the frequency domain. This is obtained by Fourier time transforming Eq. 1 to yield

$$(\nabla^2 + k^2)\mathbf{E}(x, y, z, \omega) = 0. \quad (2)$$

This is called the *Helmholtz equation* where \mathbf{E} is now a function of the angular frequency ω , equal to $2\pi f$, where f is frequency in hertz (Hz). The factor k is called the complex *propagation "constant"* or *wave number* in the medium,

$$k = \omega \left[\left(\epsilon - i \frac{\sigma}{\omega} \right) \mu \right]^{1/2}. \quad (3)$$

The corresponding wave and Helmholtz equations for the vector \mathbf{H} field are exactly as in Eqs. 1 and 2 upon substitution of \mathbf{H} for \mathbf{E} . Some researchers use the magnetic induction, \mathbf{B} , instead of \mathbf{H} via the constitutive relation $\mathbf{B} = \mu\mathbf{H}$.

We are now prepared to state the two major assumptions of the MT method. These are:

• *Quasistatic approximation*

The *quasistatic approximation* results from assuming that the σ term in k (Eq. 3) dominates over the ϵ term. That is, $\sigma \gg \omega\epsilon$. Physically, this states that electrical *conduction currents* are always very much larger than electrical *displacement currents*. Conduction currents are the familiar type as in household wiring which give rise to so-called ohmic loss or heating. Displacement currents are loss-free, temporal variations in \mathbf{E} fields which explain how an EM field (e.g., light) can propagate through a vacuum. The quasistatic approximation states that the Earth behaves as a *good conductor (poor insulator)* at the frequencies used in MT. An important consequence of the quasistatic approximation is that the complex propagation constant, k , now has real and imaginary parts of identical magnitude, i.e.,

$$\begin{aligned} k &= (-i\sigma\mu\omega)^{1/2} = (\sigma\mu\omega)^{1/2} e^{-i\pi/4} \\ &= \left(\frac{\sigma\mu\omega}{2} \right)^{1/2} - i \left(\frac{\sigma\mu\omega}{2} \right)^{1/2}. \end{aligned} \quad (4)$$

The wave equation (Eq. 1) now has only a first partial time derivative term. Physically, it becomes a *diffusion equation* of the same form that governs the diffusion of heat through a solid. Electrical conductivity in the Earth measured by MT is mainly due to ionic fluids such as saline water or magma. The dominant conduction currents proceed by the diffusion of ions through these fluids.

• *Normally incident plane wave approximation*

In the above preliminary discussion of MT source fields, it was stated that the Tikhonov-Cagniard model assumes that a plane wave is incident upon the Earth's surface. We now add the requirement that the plane wave be normally incident. This is certainly not true of waves from all sources which are superimposed to form the resultant at a given measurement site at a given time. However, because the Earth is such a good conductor (i.e., the quasistatic approximation holds), all waves, irrespective of their incoming directions are refracted very nearly vertically (normally) into the Earth. This condition, which is the essence of Madden and Nelson's (1964) defense of the Tikhonov-Cagniard model, validates the second assumption and greatly simplifies computer modeling of the MT response of the Earth.

3E.3.1. Homogeneous half-space

With a plane wave normally incident on a homogeneous half-space, the \mathbf{E} and \mathbf{H} fields are constant in direction and magnitude over planes perpendicular to the vertical, downward $+z$, direction of propagation. Taking \mathbf{E} in the x direction and \mathbf{H} in the y direction, the Helmholtz equation becomes an ordinary differential equation with solution

$$E_x(z) = E_0 e^{z/k}. \quad (5)$$

Here, E_0 is a constant which is the magnitude of E_x at $z = 0$. The minus sign is chosen in the exponent to insure that the fields decrease with propagation in the $+z$ direction in the Earth. Therefore, in a ho-

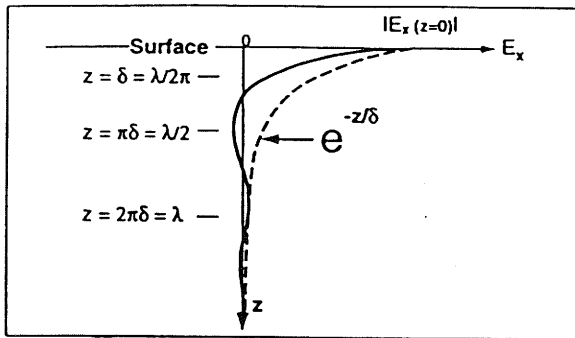


Fig. 3E-3. Exponential attenuation of sinusoidal variation of E_x as a function of propagation in the $+z$ direction. E_x magnitudes are approximately 37%, 4%, and 0.2% of the surface value at depths of a skin depth, δ , a half wavelength, $\lambda/2$, and one wavelength, λ , respectively.

homogeneous medium both the E and the H fields decrease exponentially, and at a depth equal to $1/|\text{Im}k|$ the field amplitudes are reduced to $1/e$ of their values at $z = 0$. This depth, where the field decreases to about 37% of the surface value, is called the *skin depth*, δ ,

$$\delta = \sqrt{\frac{2}{\sigma\mu\omega}} \quad (6)$$

In practical units, this equation becomes

$$\delta \approx 0.5\sqrt{\rho T} \quad [\text{km}] \quad (7)$$

after substituting $4\pi \times 10^{-7}$ henries/m for μ_0 and $\omega = 2\pi/T$, where T is the period of the incident field. SI units are used on the right side of Eq. 7, i.e., ρ in ohm-m and T in s, but the resulting units of δ are km. The skin depth, Eq. 7, is probably the most widely employed practical equation in MT since it is used to give a rough estimate of the depth of exploration. However, the skin depth equation is strictly true only for a homogeneous half-space and the real Earth is never so simple. Figure 3E-3 illustrates the spatial attenuation expressed by the skin depth and how δ relates to the wave length, λ , of the downward propagating wave. Since the real and imaginary parts of k have equal magnitudes (Eq. 4), and $\text{Re} k = 2\pi/\lambda$ for any propagating wave, this means that $\lambda = 2\pi\delta$. Furthermore, since the *phase velocity* of a propagating wave is defined as $v = \lambda f$, then v is equal to $2\pi\delta f$. Shortly, some representative

values for δ , λ , and v will be calculated, but first we consider the "trick", a parameter called the characteristic impedance, that allows the MT method to work.

As mentioned earlier, it is the spectral (frequency domain) ratios of the fields that are invariant (stochastically stationary) in MT. These ratios are the MT response of the Earth, and in the case appropriate to Eq. 5, we define the *characteristic impedance*, Z , of a medium as the spectral ratio $E_x(\omega)/H_y(\omega)$. Since the dimensions of E and H are V/m and A/m, respectively, we see that this spectral ratio has units of impedance, namely ohms. Using the expression for E_x (Eq. 5) and Maxwell's "curl-of- E " equation (i.e., Faraday's law) with an $\exp(+i\omega t)$ time dependency yields

$$Z(\omega) = \frac{E_x(\omega)}{H_y(\omega)} = \frac{\omega\mu_0}{k} \quad (8)$$

The characteristic impedance of free space ($\sigma = 0$, $\mu_0 = 4\pi \times 10^{-7}$ H/m, and $\epsilon_0 = (1/36\pi) \times 10^{-9}$ F/m), is the well-known result, $Z_0 = (\mu_0/\epsilon_0)^{1/2} \sim 376.6$ ohms. It is also very illustrative to calculate the characteristic impedance and other parameters for a typical MT situation on a continental land surface. Consequently, with $T = 100$ s and $\rho = 100$ ohm-m, Eqs. 7, 8, and subsequent discussion following Eq. 7 yield

$$\text{Re } Z = \text{Im } Z \sim 0.002 \text{ ohms}$$

$$\delta \sim 50 \text{ km}$$

$$\lambda \sim 310 \text{ km}$$

$$v \sim 3 \text{ km/s.}$$

At this same frequency the wavelength in free space is 3×10^7 km, or over 2000 times the diameter of the Earth!

We now explore the useful extensions of the concept of characteristic impedance to surface measurements where the Earth is homogeneous, 1-D, and finally, multi-dimensional.

3E3.2. Measurements at the surface of a homogeneous half-space

Figure 3E-4a schematically depicts a plane wave normally incident upon a homogeneous half-space; the wave number k can be considered as a vector

pointed in the direction of propagation. Superscripts i , r , and t denote incident, reflected, and transmitted \mathbf{E} and \mathbf{H} fields, respectively. Applying the boundary conditions that tangential \mathbf{E} and \mathbf{H} fields must be continuous across the boundary (surface of the Earth) it is straightforward (e.g., Ward and Hohmann, 1988) to show that the *transmission coefficient* is given by

$$T(\omega) = \frac{E_x^t}{E_x^i} = \left(\frac{2Z_1}{Z_0 + Z_1} \right), \quad (9)$$

and the *reflection coefficient* is

$$R(\omega) = \frac{E_x^r}{E_x^i} = \left(\frac{Z_1 - Z_0}{Z_1 + Z_0} \right). \quad (10)$$

Z_0 and Z_1 are the *characteristic impedances* of free space and the homogeneous half-space, respectively. Similar equations can be derived for the transmitted and reflected \mathbf{H} fields. For example, the reflection coefficient for the \mathbf{H} field is $\{(Z_0 - Z_1)/(Z_0 + Z_1)\}$. Reflection and transmission coefficients are very important because they describe the amplitude and phase of the reflected and transmitted fields. Those familiar with linear systems will recognize Eq. 9 and Eq. 10 as the frequency domain representations of a linear system in which $T(\omega)$ and $R(\omega)$ take on the roles of *system response functions* or *transfer functions*. Note, also, that $Z(\omega)$ in Eq. 8 is a system response function relating an input $H_y(\omega)$ to an output $E_x(\omega)$. Because MT measurements are made at the surface of the Earth we need to calculate the total \mathbf{E} and \mathbf{H} fields at $z = 0$. This can be done using the field representations either above (medium 0) or below (medium 1) the surface and letting $z = 0$. Of course, the total \mathbf{E} or \mathbf{H} fields above $z = 0$ have both an incident and reflected component. The result of these manipulations when expressed as the ratio E/H at $z = 0$ is called the *surface impedance*, Z_s ,

$$Z_s = \frac{\text{Total } E_x \text{ at } z = 0}{\text{Total } H_y \text{ at } z = 0} = Z_1. \quad (11)$$

This important result states that the surface impedance of a homogeneous half-space equals the characteristic impedance of the medium. The surface impedance is a complex function of frequency, and applying Eqs. 3 and 8, we find

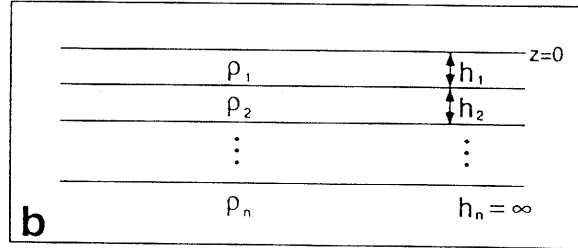
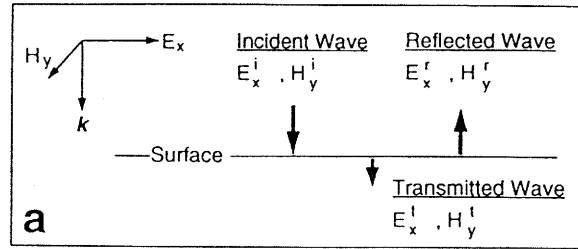


Fig. 3E-4. (a) Normally incident, reflected, and transmitted, plane waves at surface of a homogeneous half-space. E_x , H_y , and the vector propagation "constant", k , form a right-handed orthogonal set. (b) N -layered, 1-D Earth model.

$$\begin{aligned} Z_s &= \left\{ \frac{\omega \mu_0 \rho}{2} \right\}^{1/2} (1 + i) \\ &= (\omega \mu_0 \rho)^{1/2} e^{i\pi/4} \\ &= |Z_s| e^{i\pi/4}. \end{aligned} \quad (12)$$

It is customary to express surface impedance in terms of its phase, ϕ_s , and another quantity called the *apparent resistivity*. Solving for ρ in Eq. 12, a complex quantity is avoided by defining a real quantity, the *apparent resistivity*, ρ_a , as

$$\rho_a = \frac{1}{\omega \mu_0} |Z_s|^2. \quad (13)$$

The *apparent resistivity*, ρ_a , and the *phase of the surface impedance*, ϕ_s , as functions of frequency (or period) are the MT response parameters most commonly used in data presentations and interpretations.

For the case of a homogeneous half-space, these quantities are equal to the true resistivity, ρ and an impedance phase of 45° (from Eq. 12).

Physical understanding of electromagnetic reflection and transmission phenomena is enhanced by considering the approximate \mathbf{E} and \mathbf{H} relationships at the surface of a homogeneous half-space with Earth-like properties. The characteristic impedance of the Earth (~ 0.002 ohms in the sample calculation above) is very much smaller than that of the overlying atmosphere (nearly free space at 376.6 ohms). In this case, the reflection coefficient (Eq. 10) is nearly equal to -1 . A reflection coefficient of -1 means that there is total reflection with a phase change of π ; therefore, there would be total cancellation of the incident electric field. If this were exactly the case, there would be zero transmission ($T = 0$) and the MT method would be of no value for probing the Earth. Similar manipulation of the equations as done here for \mathbf{E} fields can be done for \mathbf{H} fields, yielding the result that the reflection coefficient for \mathbf{H} (given the discussion following Eq. 10) is nearly $+1$. This means that the total \mathbf{H} field at the surface of a homogeneous half-space is nearly twice the amplitude of the incident \mathbf{H} field. With the \mathbf{E} field approaching zero and the \mathbf{H} field twice its incident value at the surface of the Earth, it is not surprising that the ratio of the two (the surface impedance) is a very small quantity.

3E.3.3. Layered earth

The surface impedance of an arbitrary n -layered, 1-D earth (Fig. 3E-4B) can be found by solving the $2n$ equations obtained by applying the boundary conditions on continuity of tangential \mathbf{E} and \mathbf{H} fields at n interfaces (e.g., Wait, 1970). The important features of this solution can be gleaned by examining the simplest case where $n = 2$. In this situation the surface impedance is given by

$$Z_s = Z_1 \frac{Z_2 + Z_1 \tanh(ik_1 h_1)}{Z_1 + Z_2 \tanh(ik_1 h_1)} \quad (14)$$

The apparent resistivity is, as always, given by Eq. 13. The response (ρ_a and ϕ_s as functions of T) for this case are directly dependent on the behavior

of the \tanh functions. There are four asymptotic relations that contain the essential physics of the response. These are:

1. For *high* frequencies (*short* periods) and/or *large* h_1 , the response is that of the *top* layer. This can be seen by noting that $\tanh(ik_1 h_1) \rightarrow 1$, and Eq. 14 becomes $Z_s \sim Z_1$ so $\rho_a \rightarrow \rho_1$.

2. For *low* frequencies (*long* periods) and/or *small* h_1 , the response is that of the *bottom* layer, i.e., the basement. That is, $\tanh(ik_1 h_1) \rightarrow 0$, and Eq. 14 becomes $Z_s \sim Z_2$ so $\rho_a \rightarrow \rho_2$.

The remaining two asymptotic relations require us to make the so-called "*thin-layer*" approximation. This approximation hinges on the smallness of the argument $ik_1 h_1$ of the \tanh function so that the function can be replaced simply by its argument. The product $k_1 h_1$ is small if the skin depth ($\delta_1 = 1/\text{Im } k_1$) is large compared to h_1 . Thus, the thickness of a thin layer is small compared to its skin depth, and since $\delta = 2\pi\lambda$, a thin layer is one that is thin compared to the wavelength in the layer. *This approximation is virtually always obeyed at long periods in MT.* Applying these limits to Eq. 14 yields:

3. For *highly conductive basement*, a *thin resistive upper layer* ($\rho_2 \ll \rho_1$) is manifested by its *thickness only*, independent of its exact electrical properties. Mathematically, as $\rho_2 \rightarrow 0$, $|Z_2| \ll |Z_1|$, and

$$Z_s \approx i\omega\mu_0 h_1, \quad (15)$$

with $\rho_a \approx \omega\mu_0 k_1^2$. So ρ_a depends only on the value of h_1 , the thickness of the layer overlying the conductive basement.

4. For *highly resistive basement*, a *thin conductive upper layer* is manifested by its h/ρ quotient only (S_1 in this case). *Neither ρ or h can be resolved separately.* Mathematically: as $\rho_2 \rightarrow \infty$, $|Z_2| \gg |Z_1|$ and Eq. 14 reduces to

$$Z_s \approx \omega\mu_0 \frac{1}{ik_1^2 h_1} = \frac{1}{S_1}, \quad (16)$$

with $\rho_a \approx 1/\omega\mu_0 S_1^2$. S_1 defines the *conductance* of the layer, which is h_1/ρ_1 . That is, when $\rho_2 \gg \rho_1$, ρ_a depends on the h_1/ρ_1 quotient or the conductance of the layer overlying the resistive basement.

It is very important to note that points 3 and 4 above not only apply to the first layer of a two-layer sequence; they apply to highly conductive and highly resistive layers *anywhere* in an arbitrary, layered

sequence as long as the buried layers are thin. This simple fact provides enormous practical limitations on the resolution of MT measurements. Indeed, only when the layers are thick can we separate ρ and h in the conductive case and resolve ρ in the resistive case.

Plots of $\log \rho_a$ and linear ϕ_z versus $\log T$ (called *MT sounding curves*) are the most widely used presentations of MT data, and are the recommended plotting conventions (Hobbs, 1992). Figure 3E-5 illustrates the asymptotic relations 1 through 4 above for two-layer models where the basement is either perfectly resistive or perfectly conductive. In both cases, ρ_a curves are asymptotic at short periods to ρ_1 , the true resistivity of the top layer. The oscillations in the curves at intermediate periods are due to constructive and destructive interference of waves reflected from the top and bottom of the first layer. This is a highly attenuated version of what in optics literature is called "the quarter-wave effect." This phenomenon is well-understood in the MT case (e.g., Zhdanov and Keller, 1994), yet it was improperly attributed to an "artifact" by Spies and Eggers (1986). The lack of true one-dimensionality in the real Earth and measurement errors result in these oscillations being rarely observed in actual MT field data.

Rewriting the apparent resistivity relations given after Eqs. (15) and (16) in terms of period, T , and taking logarithms, we have

$$\log \rho_a = -\log T + \log(2\pi\mu_0 h_1^2), \quad (17)$$

and

$$\log \rho_a = +\log T - \log(2\pi\mu_0 S_1^2). \quad (18)$$

These are the logarithmic representations of asymptotic relations 3 and 4 above. Eqs. (17) and (18) are clearly equations of straight lines on log-log MT sounding curves with slopes equal to -1 and $+1$, respectively. Thus, the sounding curves in Figure 3E-5 have a slope of -45° when the basement is highly conductive and a slope of $+45^\circ$ when the basement is highly resistive. These straight lines in MT sounding plots were named "*h-lines*" and "*S-lines*", respectively, by Russian researchers (Berdichevsky and Dmitriev, 1976). These descending and ascend-

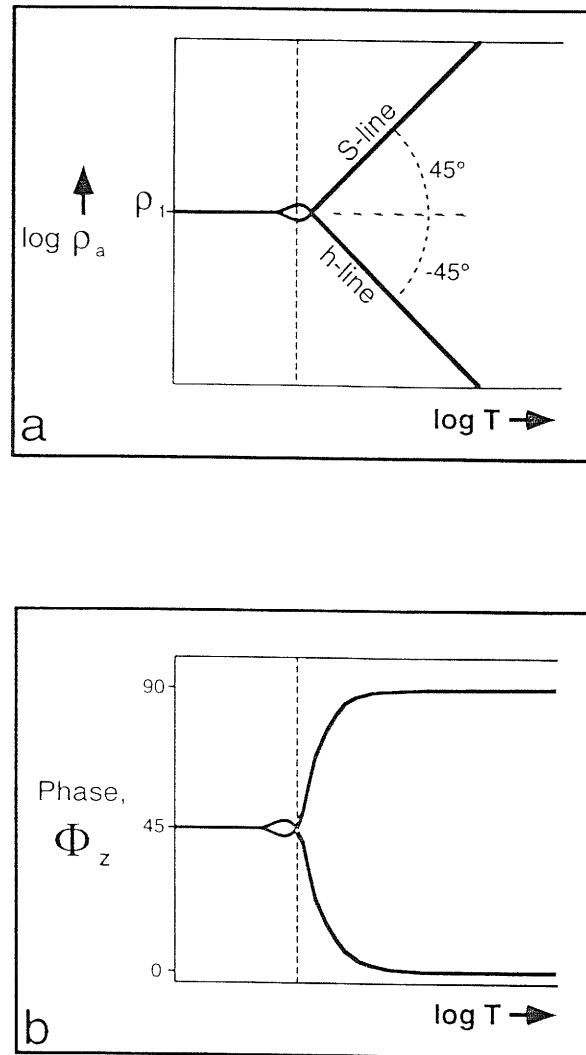


Fig. 3E-5. Two-layer MT sounding curves of (a) log apparent resistivity, ρ_a and (b) impedance phase, ϕ_z versus log period, T . Shown are the limiting cases of perfectly resistive and perfectly conductive basement which produce S-line and h-line, respectively. All other two-layer MT sounding curves would lie within these limiting cases.

ing branches can be used directly to calculate h_1 , the depth to the conductive basement, and the conductance, S_1 , above a resistive basement using

$$h_1 = \left(\frac{T\rho_a}{2\pi\mu_0} \right)^{1/2} \approx 357 (T\rho_a)^{1/2} \quad [\text{m}], \quad (19)$$

and

$$S_1 = \left(\frac{T}{2\pi\mu_0\rho_a} \right)^{1/2} \approx 357 \left(\frac{T}{\rho_a} \right)^{1/2} \quad [\text{S}]. \quad (20)$$

Convenient coordinate values at which to apply Eqs. 19 and 20 on actual ρ_a sounding curves are at $\rho_a = 1$ ohm-m, which means that observed h and S trends must sometimes be extrapolated.

Although the above relations are derived for a simple two-layer Earth, it is of utmost importance to appreciate that these relations hold approximately for highly conductive or highly resistive layers no matter how many overlying layers there are. This means that steeply descending branches ($\sim h$ -lines) can be used to calculate the *total depth* to any highly conducting layer. Similarly, steeply ascending branches ($\sim S$ -lines) can be used to calculate the *total conductance* above any highly resistive layer, i.e., $h_1/\rho_1 + h_2/\rho_2 + \dots$. In practice, a highly conductive layer closely produces an h -line when its conductance is very much greater than the total conductance of all overlying layers. A consequence of this observation is the so-called *screening effect*, i.e., the response of highly conductive layers, at the surface or at depth, will prevent the detection of deeper conductive occurrences unless they are of much greater conductance than the overlying layers. A resistive layer closely produces an S -line when its thickness is very much greater than the total thickness of all overlying layers. Thus, we are again reminded that a thin *conductive* layer is manifested by its *conductance* (point 3 above) and a thin *resistive* layer is manifested by its *thickness* (point 4 above). Later in the *Introduction to magnetotelluric interpretation* (§ 3E.4), we will illustrate the practical application of the four asymptotic relations above to both actual and synthetic data.

The complex surface impedance measured on a layered Earth can be shown to be a so-called *minimum phase function*. In this case the real and imaginary parts of Z_s are not independent; this leads to interrelations between the values of ρ_a and ϕ_z which are expressed by a Hilbert transform pair. A very useful approximate relation has been known for some

time in the Russian literature (e.g., Vanyan et al., 1967) and has been applied to MT analysis by Boehl et al. (1977). It is

$$\phi_z(T) \approx \frac{\pi}{4} - \frac{\pi}{4} \frac{d(\log \rho_a)}{d(\log T)}. \quad (21)$$

Applying this relation, we expect the phase of Z_s to be 45° at maxima and minima (and flat portions) of ρ_a log-log sounding curves. The impedance phase is 90° and 0° , corresponding to an h -line and an S -line, respectively. These features are evident in the ϕ_z sounding curves presented in Figure 3E-5. The failure of the relationship in Eq. (21) to hold (including impedance phase values outside the 0° to 90° range) is often taken as evidence for a three-dimensional (3-D) earth. The relationship (Eq. 21) seems to hold for most (perhaps all) two-dimensional (2-D) structures, although we are not aware of any proof of this assertion.

3E.3.4. Multi-dimensional earth

At the surface of a multi-dimensional (2-D or 3-D) earth or an anisotropic 1-D earth, the simple linear relation between E_x and H_y given in Eq. (11) no longer holds. The Tikhonov-Cagniard model needs revision. A solution to this dilemma was proposed by Madden and Nelson (1964) who postulated that the E_x and E_y fields depend on both the H_x and H_y fields. That is,

$$\begin{aligned} E_x(\omega) &= Z_{xx}(\omega)H_x(\omega) + Z_{xy}(\omega)H_y(\omega) \\ E_y(\omega) &= Z_{yx}(\omega)H_x(\omega) + Z_{yy}(\omega)H_y(\omega) \end{aligned} \quad (22)$$

or in tensor notation

$$\begin{bmatrix} E_x \\ E_y \end{bmatrix} = \begin{bmatrix} Z_{xx} & Z_{xy} \\ Z_{yx} & Z_{yy} \end{bmatrix} \begin{bmatrix} H_x \\ H_y \end{bmatrix} \quad (23)$$

or,

$$\mathbf{E} = \overline{\mathbf{Z}}\mathbf{H}.$$

Here, the four impedance elements form a 2 by 2 *impedance tensor*, $\overline{\mathbf{Z}}$. The field relationships of Eqs. (22) and (23) are still linear, but now each equation represents a two-input/single-output linear system (Reddy and Rankin, 1974). But, an immediate problem arises when attempting to solve Eq. (22) for the

four impedance values. Namely, the system is underdetermined since there are only two equations in four unknowns (Z_{xx} , Z_{xy} , Z_{yx} , Z_{yy}).

The four impedance elements can be determined if one can obtain four independent equations of the form of Eq. (22). This can be accomplished if two different source polarizations are used. In practice, however, because both \mathbf{E} and \mathbf{H} fields contain noise, it is statistically desirable to have many polarizations contributing to the recordings. This allows averaging to reduce the effects of noise. The result is an overdetermined system since there are now more equations than unknowns. Sims et al. (1971) developed techniques to derive least-squares estimates of the tensor impedance elements that minimize the sums of the squared differences between the measured and predicted \mathbf{E} fields.

The main problem with impedance elements estimated in this manner is that they contain autopowers (products of identical field components, one a complex conjugate) that are always biased by measurement noise. This problem can be reduced considerably by a technique called *remote reference MT* first suggested by Gamble et al. (1979). Remote reference MT uses H_x and H_y fields recorded simultaneously at two separate sites, one called the base and the other called the remote site. A substitution of the remote complex conjugate magnetic components for the base complex conjugate magnetic components can now be made when solving the impedance equations. This works well provided the desired MT signal is correlated between the base and remote sites but the noise is not; this is often the case between sites separated by only a few kilometers. For example, noise caused by wind vibrating the sensors may be totally different at the two sites while the MT signal due to large-scale ionospheric sources is highly correlated over large distances. In a recent MT survey in Italy, an electric train power distribution system produced noise correlated over tens of kilometers so the base and remote sites had to be separated by hundreds of km. Nevertheless, the desired MT signals were correlated testifying to the validity of one of the basic MT assumptions, that of normally incident plane waves.

3E.3.5. Two-dimensional earth

Now consider the MT response of a two-dimensional earth. Taking the invariant (or strike) direction to be the y-coordinate of a 2-D earth will define the *geoelectric strike direction*. For this coordinate choice, $\partial/\partial y = 0$, and Maxwell's electromagnetic equations separate into two independent modes or polarizations. The component of the electric field, E_y , parallel to the *geoelectric strike direction* defines *E-polarization*; the component of electric field perpendicular to the *geoelectric strike direction* defines the *H-polarization*. The terms E- and H-polarization are those recommended by the international EM induction community (Hobbs, 1992). Alternative specifications of *transverse electric (TE)* and *E-parallel* are also commonly used to designate E-polarization. These terms relate to the orientation of E_y transverse (perpendicular) to the *geoelectric plane* of symmetry and its parallel relationship to the *geoelectric strike direction*, respectively. *Transverse magnetic (TM)* and *H-parallel* are corresponding terms used interchangeably for H-polarization. The E- and H-polarizations each has only three EM field components. For E-polarization, where E_y is assumed, H_x and H_z are derived from Maxwell's equations. Correspondingly, for H-polarization, where H_y is assumed, E_x and E_z are derived from Maxwell's equations.

In the perfect 2-D case, only two impedances are needed to completely describe the tensor impedance. That is, the 2 by 2 impedance tensor in Eq. (23) reduces to

$$\bar{\mathbf{Z}} = \begin{bmatrix} 0 & Z_{yx} \\ Z_{yx} & 0 \end{bmatrix} \quad (24)$$

where

$$Z_{yx} = -E_y/H_x, \quad Z_{xy} = E_x/H_y, \quad (25)$$

and the diagonal elements of the impedance tensor are zero.

As in Eqs. 22 and 23, the first subscript refers to the electric field component; therefore, Z_{yx} and Z_{xy} are the impedance elements for the E- and H-polarizations, respectively. The corresponding apparent resistivities are calculated using Eq. 11 where Z_{yx} and Z_{xy} are substituted for Z_z .

In the 1-D (or homogeneous) case the impedance response of the Earth is described by two numbers (parameters) at each sample period since Z_z is a complex quantity. The two separate complex impedance elements in the 2-D case (Eq. 25) yield four parameters in the impedance description. Actually, there are five parameters since the orientation of the rectangular coordinate system must also be included.

In actual field practice, the orthogonal measuring axes (Fig. 3E-2) rarely coincide with directions exactly parallel and perpendicular to the geoelectric strike. Consequently, the coordinate system must be rotated either physically or computationally to off-diagonalize the impedance tensor to the form of Eq. 24. This is expressed computationally by a standard coordinate transformation or rotation by some angle. If the Earth were perfectly two-dimensional, there would be a specific angle where Z_{xx} and Z_{yy} would be identically zero. Since the actual Earth is never exactly two-dimensional, some other scheme must be used to determine an approximate or quasi 2-D earth geometry. Most schemes either minimize some combination of the diagonal components of the impedance tensor or maximize a combination of the off-diagonal elements, usually in a least squares sense. This analysis is often called a *Swift analysis* (Swift, 1967). For a perfectly 2-D earth, the Swift analysis yields two directions called the *principal directions*; one is the *geoelectric strike direction* and the other direction perpendicular to the strike is the *geoelectric dip direction*. In an ideal 2-D earth, identical principal directions would be calculated at all measurement sites and at all sounding periods.

The importance of the basic Swift analysis cannot be overemphasized since it has been the dominant MT processing scheme for over 25 years. The analysis always produces principal directions, but they represent quasi 2-D geoelectric strike and dip directions. In nature, the directions always vary at different periods and from site to site in violation of a perfect 2-D earth. Swift (1967) presented indices called *skew* and *ellipticity* to quantify the degree of violation. Even so, the most common presentations of MT data are those parameters appropriate for a perfect 2-D case. Namely, apparent resistivity and impedance phase are presented as functions of period for the two principal directions. These values

are designated E-polarization, TE, or E-parallel and H-polarization, TM, or H-parallel, even though such designations are strictly true only for a perfect 2-D geometry.

The rotation of the tensor impedance elements to achieve principal directions even in a 2-D situation does not actually distinguish the E-polarization direction from the H-polarization direction since there is a 90° ambiguity in the rotation. This ambiguity is eliminated by using the fact that only the E-polarization gives rise to a vertical magnetic field. Swift (1967) defined a complex parameter called the *tipper* function which describes a linear relation between the vertical and horizontal magnetic fields. Consequently, in the multi-dimensional case,

$$H_z = T_x H_x + T_y H_y . \quad (26)$$

The term, *tipper*, is ascribed to T. Madden (Vozoff, 1972) who visualized the horizontal magnetic field over a 1-D earth as being tipped into the vertical by the effects of lateral inhomogeneities. The coordinate directions of the tipper can be rotated just as the impedance tensor can be. For a 2-D earth, the tipper can thus be expressed as a function of only one principal direction, the dip direction. The easiest way to understand the concept of the tipper function is to use the "right-hand rule" as learned in introductory physics. Assuming that the right thumb points in the direction of geoelectric strike, the right-hand fingers curl in a circular manner about the thumb. The direction of the thumb is that of current (or E_y) in the strike direction. The pattern of the fingers represents both the H_x and H_z magnetic field directions set up by the current flow. Therefore, where the y-direction is the strike direction of a 2-D Earth, the current flow along strike produces the H_x and H_z magnetic fields; the tipper relation quantifies the relation between the magnetic field components. This discussion presents the essential physical nature of the E-polarization, which has only the field components E_y , H_x , and H_z . Another way of presenting the relation between the vertical and horizontal magnetic fields is to treat the tipper as a complex vector (T_x , T_y). This permits the definitions of in-phase and out-of-phase *induction vectors* or *induction arrows* (Schmucker, 1970) as functions of frequency and location.

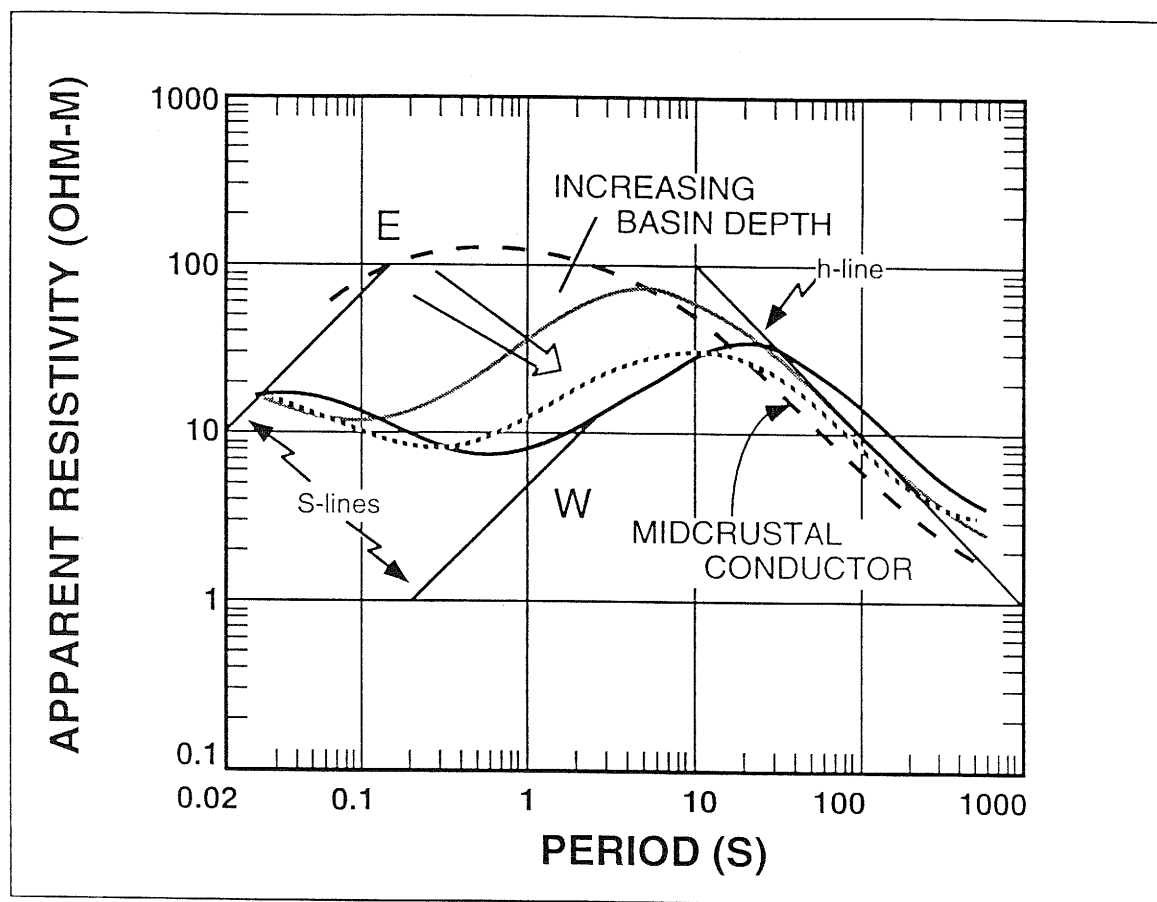


Fig. 3E-6. Sequence of E-polarization apparent resistivity versus period MT sounding curves from the Rio Grande rift. Ascending branches (near S-lines) from 0.1 to 10 s period indicate increasing basin depth from east to west; h-lines at periods >10 s mark the response of a midcrustal conductor. The h-line drawn yields a depth of 11 km to this conductor; the S-lines drawn yield a range of basin conductance from 15 to 200 S.

3E.4. Introduction to magnetotelluric interpretation

3E.4.1. One-dimensional interpretation

The principles of 1-D MT interpretation are detailed in the previous discussion in *Layered earth* (§ 3E.3.3) under the Basic magnetotelluric principles section. These principles are illustrated in Figure 3E-6, which contains four smoothed MT sounding curves across a portion of the Rio Grande rift near Santa Fe, New Mexico (Jiracek et al., 1987; Biehler

et al., 1991). The very fact that the curves vary across the rift basin violates the 1-D assumption. But, as shown in the next section, some multi-dimensional MT curves (especially E-polarization curves from a 2-D conductive surface environment) may yield a reasonable 1-D estimate of the vertical section beneath a recording site. The curves presented in Figure 3E-6 are such examples. There are four obvious layers expressed in these soundings. Data at periods shorter than 1 s reflect an increasingly conductive (lower resistivity) water-saturated, basin-fill with a fresh water layer overlying a saline water zone. Be-

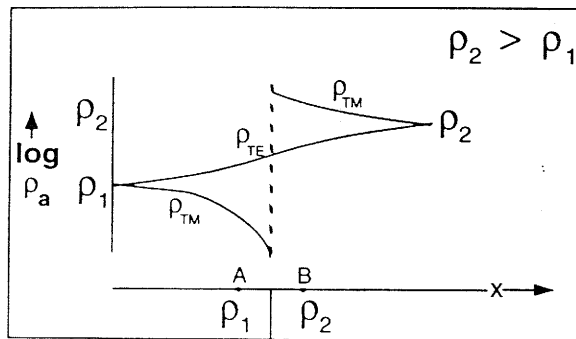


Fig. 3E-7. Variation of TE and TM apparent resistivities versus distance at a single period across a vertical contact. ρ_{TE} varies smoothly within the range of ρ_1 and ρ_2 ; ρ_{TM} is discontinuous with values far outside the range of ρ_1 and ρ_2 .

low these two layers is a resistive (>100 ohm-m) basement of relatively dry granitic composition, like that of the mountains bounding the rift (Biehler et al., 1991). Finally, there is a very prominent midcrustal conductive zone whose bottom is not resolved by the 800 s period data. Applying the four asymptotic relations from the *Layered earth* section we find: (1) The top layer resistivity is about 20 ohm-m; (2) The deepest layer resistivity is 2-3 ohm-m; (3) The depth (using Eq. (19)) to the top of the midcrustal conductor is about 11 km using the h-line in Fig. 3E-6; and (4) The total conductance (using Eq. (20) and the S-lines drawn in Fig. 3E-6) above the resistive basement varies progressively east to west across the basin from about 15 to 200 S. Since the MT results are virtually identical at the shortest periods, i.e., the resistivity variations above the basement are laterally continuous, the change in conductance reflects increasing basin depth. The variations in the positions of the h lines revealing the midcrustal conductor are thought to arise from 3-D (along strike) variations rather than any significant changes in the depth to conductor. All of the above geoelectric features are highly consistent with seismic and gravity interpretations (Biehler et al., 1991) except for the midcrustal conductor. This strong electrical feature, which is thought to be

caused by important geochemical phenomena in the crust (section § 3E.5), is not sensed by any other geophysical method.

3E.4.2. Two-dimensional interpretation

The most important characteristics of 2-D MT apparent resistivity sounding curves are realized by understanding the variations in E- and H- polarization results on either side of a simple geoelectric contact. Figure 3E-7 depicts such a contact with ρ_1 representing the more conductive quarter-space to the left of resistive quarter-space ρ_2 . The physics of the response of this 2-D model at the two measurement sites A and B is profoundly different for the two polarizations.

E-polarization

All three EM field components in E-polarization (E_y , H_x , and H_z) are continuous across all boundaries so the fields vary smoothly across geologic contacts. Therefore, the apparent resistivity, which is proportional to E_y/H_x (Eqs. 11 and 13) is smoothly varying across a contact. Figure 3E-7 illustrates this behavior as measured at a constant arbitrary period. The ρ_{TE} curve would be sharper at arbitrarily shorter periods compared to a smoother curve at longer periods. This behavior is characteristic of the *inductive effect*, which controls the frequency response of the E-polarization. This effect depends on the time derivative of the magnetic flux (Faraday's law of induction) so it diminishes at lower frequencies. Note that the ρ_{TE} response in Figure 3E-7 does not lie outside the range defined by ρ_1 and ρ_2 .

H-polarization

In H-polarization, H_y and E_z are continuous across a contact but E_x is discontinuous. The discontinuity in E_x follows from the continuity of the normal component of the current density, J . The definition of J results in continuity of the quotient E_x/ρ in the model in Figure 3E-7. The electric field discontinuity at a contact is due to electric charge accumulation on the contact which is the underlying cause of the *galvanic effect* (Berdichevsky and Dmitriev, 1976). The galvanic effect produces the discontinuous behavior of

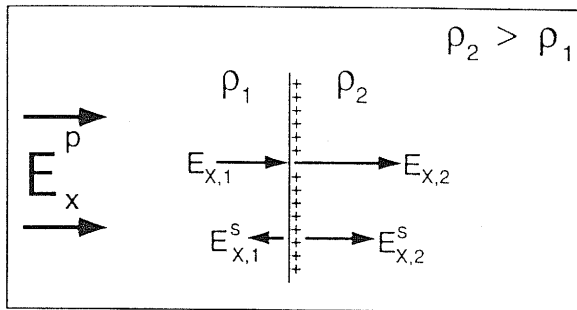


Fig. 3E-8. Primary electric field, E^p , normally incident on 2-D contact schematically showing surface charge accumulation, secondary electric fields, $E_{x,1}^s$ and $E_{x,2}^s$, and total electric fields, $E_{x,2}$ and $E_{x,1}$. The secondary electric fields from the + charges subtract from the primary field on the conductive side (ρ_1) and add to the primary electric field on the resistive side (ρ_2), resulting in $E_{x,2} > E_{x,1}$.

the ρ_{TM} results shown in Figure 3E-7 with values falling far outside the range of ρ_1 and ρ_2 . The discontinuity in ρ_{TM} ($\propto |E_x/H_y|^2$) is identical to the square of the $E_{x,2}/E_{x,1}$ discontinuity discussed above because there is no change in H_y along the surface in the 2-D case. This emphasizes the dominant role played by electric field discontinuities in H-polarization apparent resistivity responses. It can be shown (e.g., Kaufman, 1985) that electric charges form anywhere there exists a component of electric field in the direction of a change in resistivity. The charges are the source of *secondary electric fields* that modify the initial (or *primary*) electric fields. The resulting *total* (primary plus secondary) electric fields are those that appear in the continuity relations for the normal component of \mathbf{J} . Figure 3E-8 graphically shows these relations for a primary electric field perpendicular to a 2-D resistivity contrast. The secondary field directions and magnitudes on each side of the contact are schematically those required for a total field increase on the resistive side and the opposite on the conductive side of the boundary. The determination of the surface charge polarity is made by recalling that the secondary electric field directions must be consistent with the direction that a

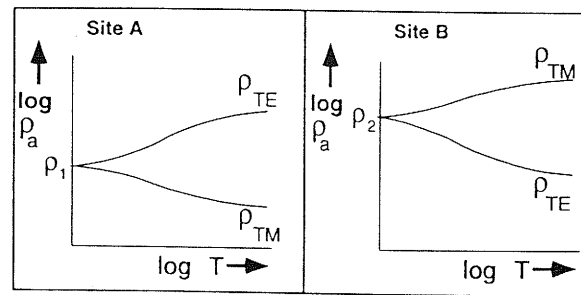


Fig. 3E-9. Schematic MT apparent resistivity sounding curves at sites A and B in Fig. 3E-7. Curve for ρ_{TE} is above that for ρ_{TM} on the conductive side of the contact and ρ_{TM} is above ρ_{TE} on the resistive side.

hypothetical positive test charge would move. Those directions are directed away from a positively charged boundary as depicted in Figure 3E-8.

In Figure 3E-7, note that at locations sufficiently removed from the contact, neither ρ_{TE} or ρ_{TM} responses sense the contact. This horizontal distance is approximately one skin depth (Vozoff, 1991). The curves sketched in Figure 3E-7 graphically present the major characteristic differences between E- and H-polarization MT apparent resistivity results. Namely, that E-polarization (TE) values plot above H-polarization (TM) results on the conductive side of a contact and, vice versa on the resistive side of a 2-D contact. This realization, along with a basic geologic knowledge of the survey area, can be of enormous value when first trying to understand MT observations.

The characteristics emphasized above at a single period, of course, transfer to the sounding curves at various measurement sites. Such apparent resistivity sounding curves for two sites, one on either side of the contact in Figure 3E-7, are presented in Figure 3E-9. Two major characteristics of these soundings are: (1) both curves converge to the true resistivities at each site location at the shortest periods, and otherwise; (2) ρ_{TE} is above ρ_{TM} on the conductive side of the contact (site A), and vice versa on the resistive side of the contact (site B).

A convenient way to display many MT sounding curves along a profile is in so-called *pseudosection* form. A pseudosection is a plot of contours of equal

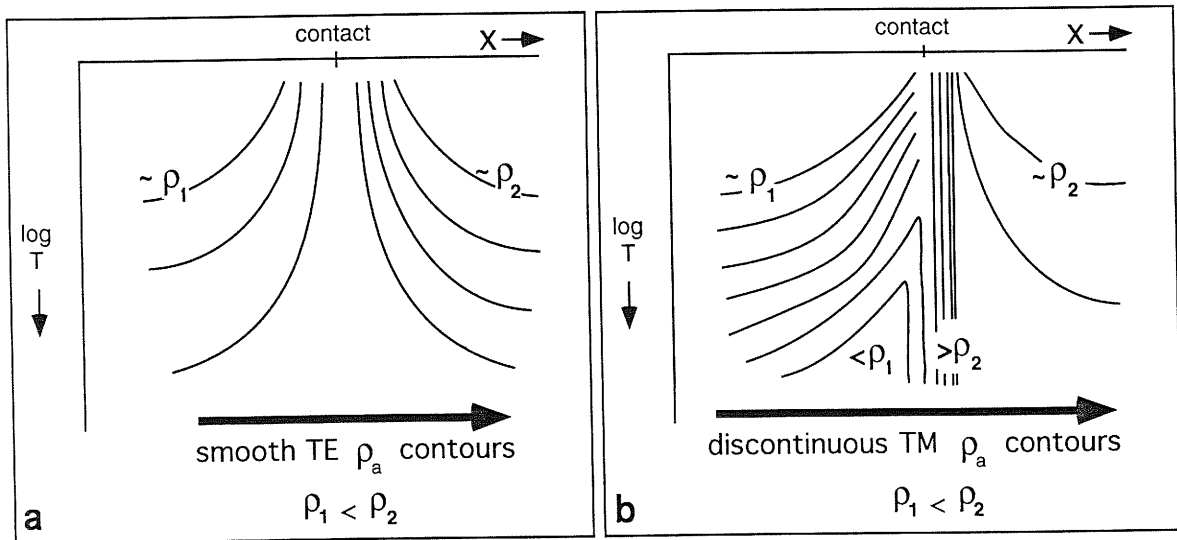


Fig. 3E-10. Representative pseudosections of (a) TE, and (b) TM, apparent resistivity (ρ_a) across a vertical contact in Figure 3E-7. Horizontal location of contact is marked by ρ_a , vertical contours especially in TM case where values are discontinuous.

apparent resistivity, or impedance phase, where the horizontal axis is linear horizontal distance (e.g., in km) and the vertical axis is the log of the period (Fig. 3E-10). Since the shorter period data plot at the top of the graph and the longer period data at the bottom, apparent resistivity pseudosections give a rough idea of the true-resistivity geoelectric section. However, the term 'pseudo' is highly appropriate for such plots since they can be very misleading. For example, the discontinuous behavior of the ρ_{TM} data across a simple contact (Figure 3E-7) plots as a false intrusive-like conductive zone on the low resistivity side of a contact (Fig. 3E-10b). Such false behavior does have a beneficial aspect since sharp vertical contours are good indicators of the positions of lateral boundaries, especially in ρ_{TM} pseudosections (Fig. 3E-10).

To illustrate the above 2-D MT considerations, a hypothetical geologic-geoelectric continental rift model depicted in Figure 3E-11 is used. Figure 3E-12 contains the MT apparent resistivity sounding curves for sites 1 and 2 at locations in the conductive basin and on a neighboring resistive flank (Fig. 3E-11), respectively. Plotting both soundings on the same graph allows a clear comparison of the two

major characteristics emphasized above. Namely, 1) the curves converge to the true resistivities (10 and

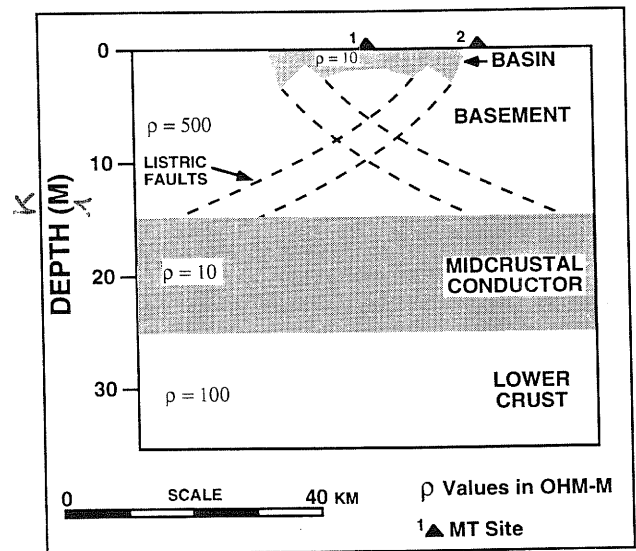


Fig. 3E-11. Hypothetical 2-D geologic-geoelectric continental rift model with conductive 10 ohm-m basin bounded by listric faults, 500 ohm-m basement, 10 ohm-m midcrustal conductor from 15 to 25 km depth, and 100 ohm-m lower crust.

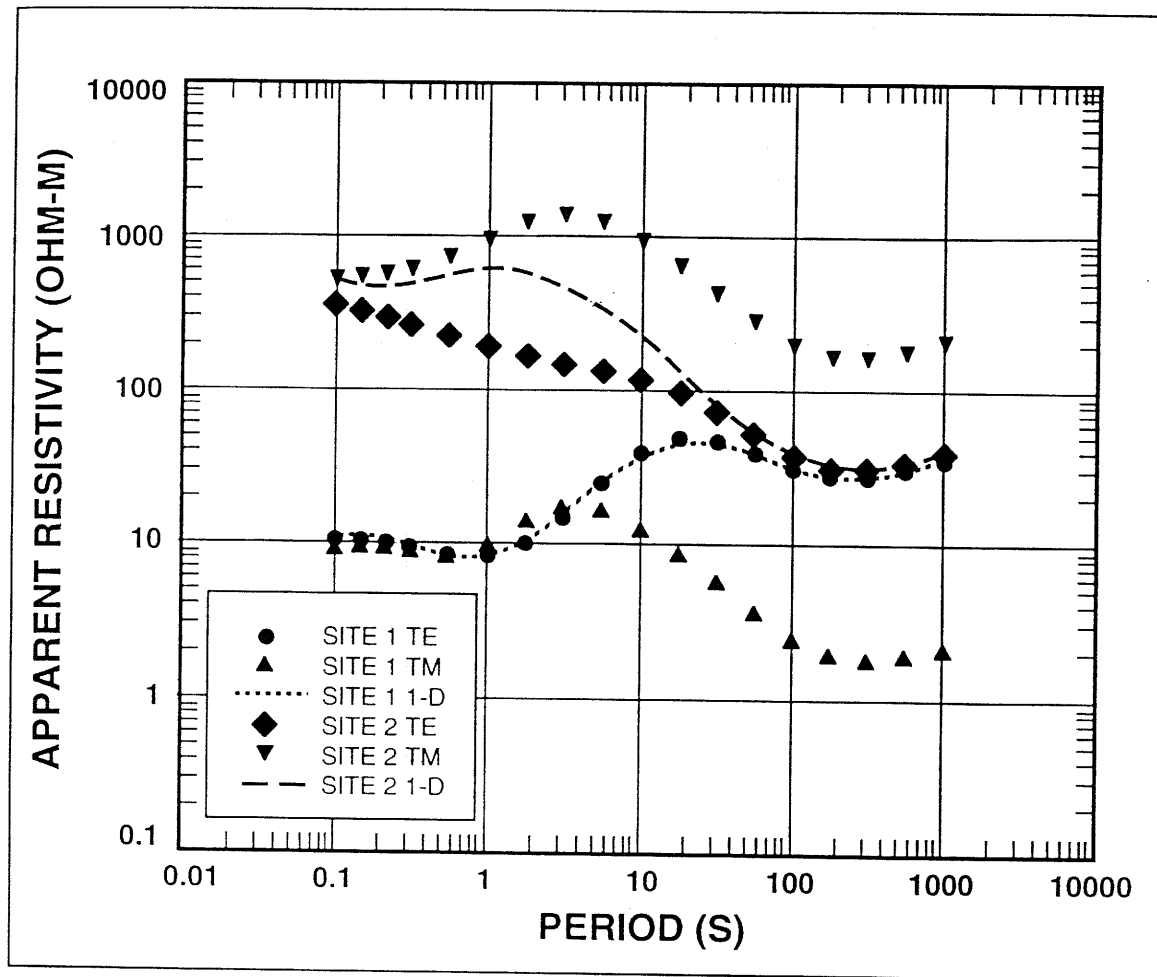


Fig. 3E-12. Synthetic apparent resistivity MT sounding curves at sites 1 and 2 within and outside the conductive rift basin shown in Fig. 3E-11. ρ_{TE} curve virtually equals 1-D curve appropriate for vertical section below conductive site 1. ρ_{TE} curve agrees with 1-D curve appropriate for vertical section below resistive site 2 only at long periods.

500 ohm-m, respectively) at the shortest periods and 2) ρ_{TE} is above ρ_{TM} at site 1 and vice versa at site 2. Imprinted on these observations are the effects of skin depth, and a 10 ohm-m midcrustal conductive zone from 15 to 25 km depth. The latter is expressed as descending branches on all curves especially from 10 to 100 s period. It is very instructive to compare the 2-D curves with the 1-D results calculated at each site as if a layered Earth with the same vertical section is assumed. These results (Fig. 3E-12) show how closely the TE curve on the conductive side (site

1 in the basin) matches the 1-D curve. This is not true for results at resistive site 2 adjacent to the basin except at the longer periods. Note that all curves in Figure 3E-12 begin to rise at the longest periods shown; this is the response to a more resistive (100 ohm-m) lower crust (Fig. 3E-11).

Although 2-D Earth models can be constructed with very complicated responses that require careful attention to vertical and horizontal skin depth considerations, the simple features discussed above are surprisingly useful in initial interpretations.

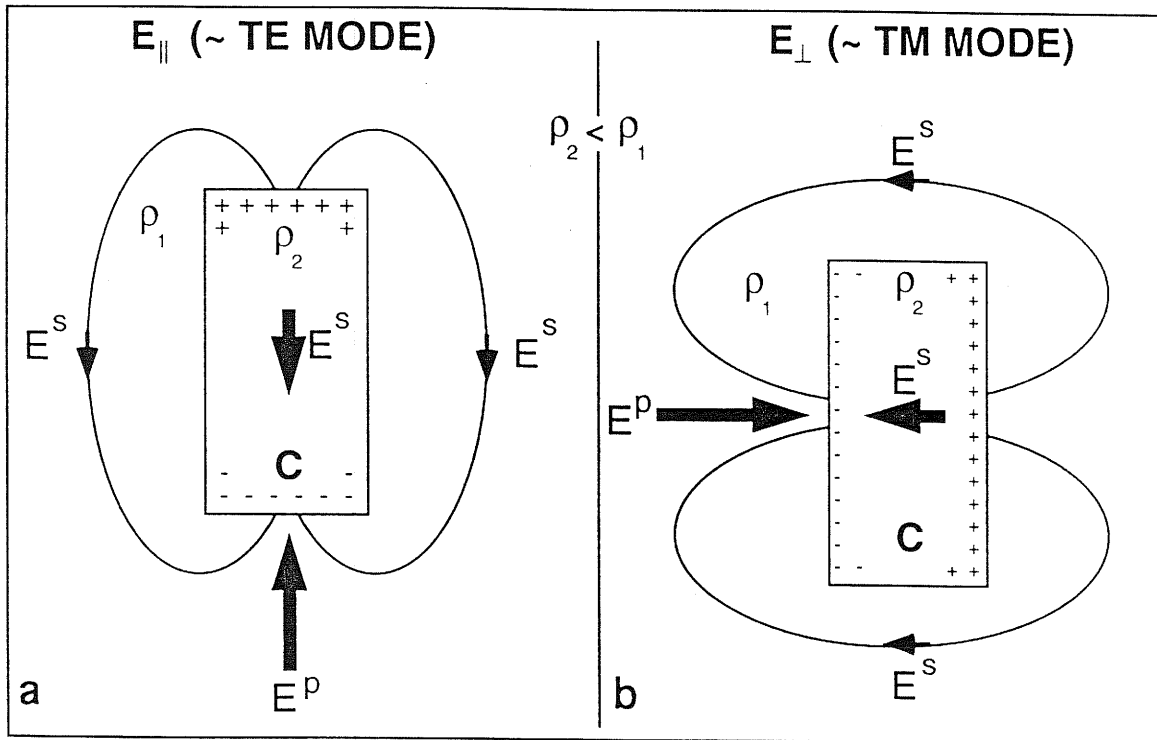


Fig. 3E-13. Plan view of primary electric field, E^P , normally incident on ends of 3-D conductive (C) body schematically showing dipolar surface charge accumulation and secondary electric fields, E^S . The secondary electric fields subtract from E^P over the conductive body and along its sides but add to E^P off the ends of the body in both the \sim TE (a) and \sim TM (b) cases. The macroscopic effect is current channeling into the conductive body (Jiracek, 1990).

3E.4.3. Three-dimensional interpretation

The MT response of 3-D Earth structures is dominated by galvanic effects because electric field components in the directions of resistivity changes occur in all directions. Now, whereas the impedance description of 1-D and 2-D Earths required 2 and 5 parameters, respectively, the 3-D Earth requires 8. These are the real and imaginary parts of each of the full 4 tensor impedance elements (Eq. 23). To illustrate the major 3-D effects, it is sufficient to present two simple examples. Both examples use 3-D rectangular blocks, one conductive and one resistive.

Electric field distortion

Figure 3E-13 presents a map view of a 3-D rectangular body that is conductive relative to a surrounding layered host. A primary electric field is sketched both parallel and perpendicular to the long axis of the body. These cases are designated E_{\parallel} and E_{\perp} , respectively, in Figures 3E-13a and 3E-13b. There are no strict designations of E-polarization and H-polarization for the 3-D case, hence, terms \sim TE mode and \sim TM mode are used in Figure 3E-13. Included schematically in the two examples in Figure 3E-13 are the galvanic charge distributions and resulting secondary electric field variations, E^S . The polarity of the charges is such to cause a secondary field opposing the primary field in the conductive

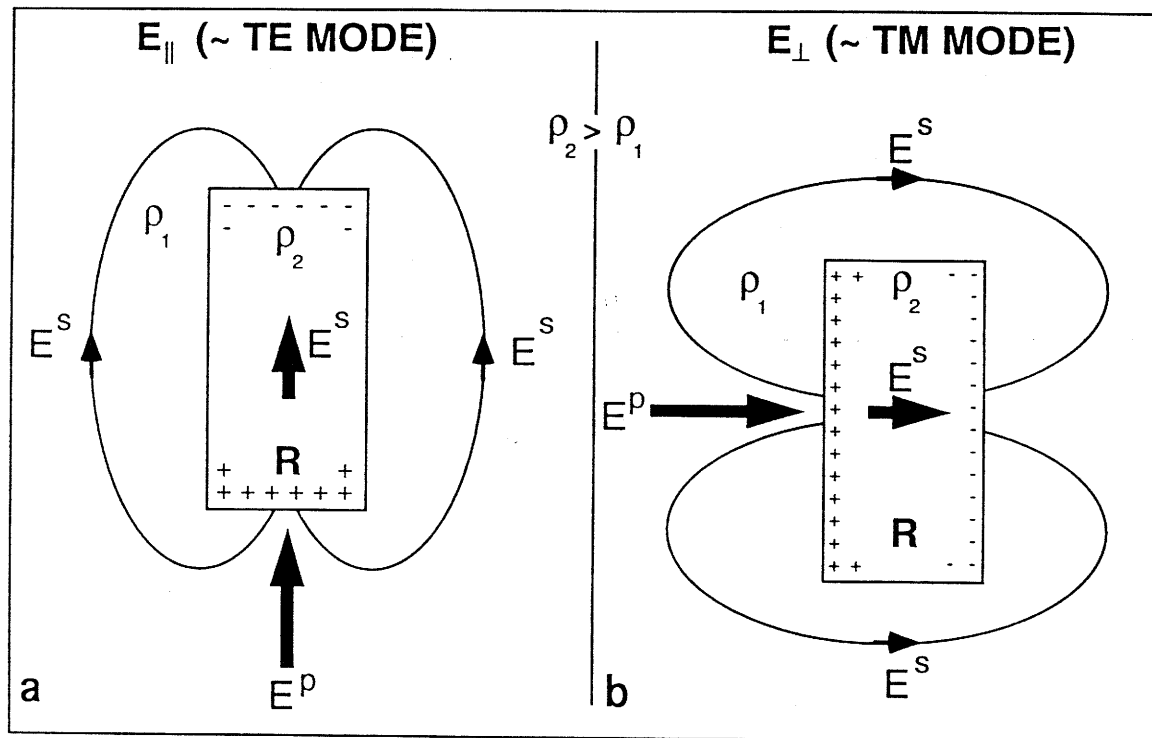


Fig. 3E-14. Plan view of primary electric field, E^p , normally incident on ends of 3-D resistive (R) body schematically showing dipolar surface charge accumulation and secondary electric fields, E^s . The secondary electric fields add to E^p over the resistive body and along its sides but subtract from E^p off the ends of the body in both the \sim TE (a) and \sim TM (b) cases. The macroscopic effect is current deflection around the resistive body (Jiracek, 1990).

body. Only then can the total electric field decrease in a conductive body as required to preserve the continuity of normal current density. Even though the total E is decreased in a conductor it is important to realize that the current is enhanced. This expected increase of current in good conductors is called *current channeling*.

For clarity, some details are omitted in Figure 3E-13 since the sketches are meant to show only the major features. The important result is that there are galvanic charges and H-polarization-like effects for both polarizations of the electric field. By simply estimating the sense of the vectorial addition of the primary and secondary electric fields depicted in Figure 3E-13, one can make a good guess of what the resulting total E field patterns will be. For ex-

ample, the total field is reduced directly over the body and along its sides, whereas the fields are enhanced off the ends of the conductor. The overall, total effect is that of current channeling into conductive inhomogeneities (Jiracek, 1990).

Figures 3E-14a and 3E-14b present the situations opposite to those in Figure 3E-13, namely those of a relatively resistive 3-D inclusion. Now the secondary field must be additive to the primary field in the resistive body. This single consideration enables the sketches in Figure 3E-14 to be made. From these it is clear that the total electric field is enhanced directly over the body and along its sides, but, it is diminished off the ends. Now the current channeling is around the outside of the resistive body, an effect called *current deflection*.

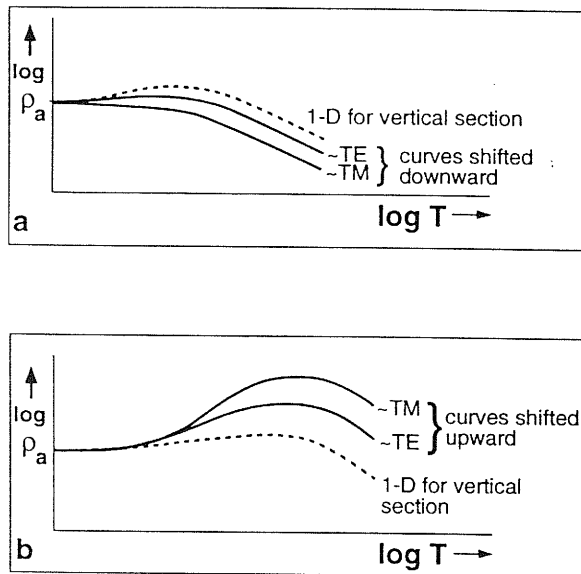


Fig. 3E-15. Schematic apparent resistivity MT sounding curves over 3-D conductive (a) and resistive bodies (b) in Fig. 3E-14 compared to curves appropriate to 1-D section in which bodies are embedded. Both \sim TE and \sim TM sounding curves are static shifted downward over the conductive body and they are static shifted upward over the resistive body.

Distortion of apparent resistivity curves

An understanding of the galvanic electric field distortions alone often enables one to estimate the surface effects on 3-D MT sounding curves even though the apparent resistivity calculation (Eq. 13) includes both the electric and the magnetic fields. This is so because the 3-D galvanic magnetic field distortion is determined by a volume integral of the current distortion, which is small for near-surface bodies of small volume. In these cases, the apparent resistivity results are dominated by electric field variations. They are shifted upward where the total electric fields are enhanced and are shifted downward where total electric fields are depressed. These observations explain why the \sim TE and \sim TM apparent resistivity curves directly over isolated conductive and resistive bodies are shifted as shown in Figures 3E-15a and 3E-15b, respectively. The results

are sketched in comparison to an apparent resistivity sounding curve appropriate to a 1-D Earth with the same vertical properties as the 3-D case. This shows that the 3-D sounding curves are shifted downward at sites located over surface conductors and upward over resistors. However, at sites off to the side of a conductive body, for example, the \sim TE curves would be shifted up and the \sim TM curves would be lowered. These conclusions follow from scrutiny of the sketches in Figures 3E-13a and 3E-13b.

Where the shifting up or down of the apparent resistivity sounding curves is frequency (period) independent, the constant shift is referred to as a *static shift*. The shift is constant or static when the primary electric field is uniform over the extent of the body, the galvanic magnetic effects are inconsequential, and the inductive (TE-like) effects are negligible. These requirements are always met for small 3-D bodies below some frequency value, therefore, above some arbitrarily long period. As frequency decreases, the increased skin depth in the host rock eventually results in a quasi-uniform charging field over the depth extent of the body. At high frequencies the field is stronger at the top of a body, therefore, the body is charged more at the top. Such a variation with frequency does not produce a static shift. Inductive effects, since they depend on a time derivative, always decrease with decreasing frequency.

The question of whether or not magnetic field galvanic distortion can be neglected depends on the overall volume of the current channeling and/or current deflection as mentioned earlier. An informed discussion of this topic has been recently presented by Chave and Smith (1994) where they confirm that such distortion is frequency dependent. Therefore, galvanic magnetic effects or significant inductive response from 3-D bodies oppose static shift. Still, it is clear to all MT practitioners that there is a surprising recurrence of static shifts in MT sounding data. In fact, static shifts are probably the leading contemporary problem in magnetotelluric processing and modeling. Therefore, it is not unexpected that many schemes have been devised to address the problem of static shift (a review of techniques appears in Jiracek, 1990). However, no method is com-

pletely successful without auxiliary data. In actual situations different static shifts from different scales of inhomogeneities in the vicinity of a measurement site all superimpose.

Several well-formulated proposals have appeared in recent years to partially address the 3-D galvanic distortion problem (e.g., Groom and Bahr, 1992; Chave and Smith, 1994). The details of these are beyond the scope of this discussion. However, since this is one of the most active research areas in MT, the main theme of these techniques is briefly presented here. Namely, the measured (distorted) impedance tensor is mathematically expressed in terms of a background (regional) impedance multiplied by tensor distortion terms. The desired regional impedance is assumed to be either 1-D or 2-D; the distortion tensors allow for 3-D electric and magnetic distortions. The latter are complex and frequency dependent; the former are real, frequency independent (static) distortions. Both distortions are location dependent. In practice, a low frequency assumption is usually invoked wherein the wavelengths inside and outside the inhomogeneities are large compared the size of the 3-D scatterer. This, and the neglect of the magnetic distortion, produces real, frequency independent electric field distortion tensor elements (Larsen, 1977; Wannamaker et al., 1984; Zhang et al., 1987; Bahr, 1988; Groom and Bailey, 1989). Galvanic (current channeling) magnetic effects have been included in 3-D MT distortion formalisms by Groom and Bailey (1991), Zhang et al. (1993), and Chave and Smith (1994). All of the tensor distortion schemes perform tensor decomposition to attempt to retrieve a pure, undistorted regional impedance tensor. Unfortunately, an indeterminacy remains for each method that requires the independent knowledge of the regional impedance tensor for at least one frequency.

3E.5. Mid-to-lower crustal conductive zones

3E.5.1. Introduction

It has been argued recently (Hyndman et al., 1993) that the deep crust is conductive everywhere. However, there is a trend for tectonically active areas to have shallower (midcrustal) conductive zones that

are better developed than in stable areas. That continental rifts have such features was recognized early on, e.g., by Schmucker (1964) in the Rio Grande rift. Jiracek et al. (1979) emphasized this observation for four rifts (Rio Grande, Baikal, East Africa, and the Rhinegraben) by concluding that they are characterized by zones of < 50 ohm-m at depths of 10–30 km. Jones (1992) summarized an additional 10 years of data and correctly states that no single conductivity model fits all rifts. In fact, there are still arguments about whether or not there is a crustal conductor directly beneath the Rhinegraben or just under its eastern shoulder (Schmucker and Tezkan, 1988; Jones, 1992; Mareschal et al., 1994). For other young continental rifts the question is not if, but why, there are conductive zones. Naturally, the next question is what are the consequences?

The question of why the mid-to-lower continental crust is conductive is truly a "hot topic" as evidenced by a barrage of recent papers on the subject. Jones (1992) has a very complete summary as do Hyndman et al. (1993). There has also been a major effort to relate the conductive occurrences with crustal seismic reflectors and refractors (Gough, 1986; Jones, 1987; Hyndman, 1988; Hyndman and Klemperer, 1989; Hyndman and Shearer, 1989; Merzer and Klemperer, 1992). The intent of this contribution to be a practical assessment of MT in a continental rift environment demands a brief review of some of these recent results. This will be done in an overview manner; the reader is strongly urged to consult the above references for more details.

3E.5.2. Sources of crustal conductors

There are really only three possible sources for crustal conductive zones. These are water, magma, and conductive minerals such as graphite. Because graphite is much more conductive ($\rho = 10^{-5}$ ohm-m; Duba and Shankland, 1982) than highly saline water (10^{-2} ohm-m minimum; Nesbitt, 1994) which is in turn more conductive than magma (about 0.5 ohm-m; Hermance, 1979), it requires much less graphite to produce a conductive zone. Temperatures in the lower crust are above the critical temperature (374°C for pure H_2O) so the term *aqueous fluid* is preferred instead of water since liquid and gaseous H_2O are

indistinguishable. After early interpretations that conductive zones, especially in rift environments, were caused solely by magma (e.g., Pedersen and Hermance, 1978; Banks and Beamish, 1979) the favored explanations have become aqueous fluids or conductive minerals, mainly graphite (Hermance and Pedersen, 1980; Jiracek et al., 1983; Jodicke, 1993; Hyndman et al., 1993; Katsube and Mareschal, 1993). As stressed by Jones (1992), there is no single cause for the enhanced crustal conductivities since different effects operate in different tectonic environments and at different depths.

For H₂O to accumulate in the crust, there must be both a source and a capping mechanism. Sources include deep circulating meteoric water, crustal devolatilization by metamorphic reactions, and fluids released from mantle derived magmas crystallizing higher up in the lithosphere. Newton (1990) emphasized that emplacement of mantle-derived magmas in the lower crust contributes greatly to the thermal and volatile budgets in highly extensional regimes such as rifts. The magma volatile content is mainly H₂O and CO₂ (Wilson, 1989), the solubility of which decrease as the magma migrates upward. The fate of ascending volatiles depends on pressure, temperature, time, and whether crustal melting or retrograde metamorphism occurs (Thompson and Connolly, 1990). H₂O is very soluble in granitic melts and retrograde metamorphism moves water into hydrated minerals that are resistive (Olhoeft, 1981). A theoretical reason to expect trapping of aqueous fluids in cracks at the brittle-ductile transition in the crust has been presented by Bailey (1990). The argument is that vertical fluid transport is rapid in the ductile crust but that it slows abruptly at the brittle-ductile transition. The resulting overpressure would induce horizontal fractures in which water would accumulate. Bailey's (1990) hypothesis is especially appealing since the coincidence of the depth to the top of crustal conductive zones and the brittle-ductile transition has been reported by several studies (e.g., Jiracek et al., 1983; 1987; Hyndman et al., 1993). However, Bailey's (1990) mechanism would operate most effectively where the principal regional stress is horizontal (compressional) rather than vertical as it is in extensional rift environments.

The question of whether graphite, or other conductive minerals exist in the deep crust must also address the sources and accumulation processes (Hyndman et al., 1993). The source of graphite is usually thought to be from the reduction of CO₂-rich fluids. CO₂ itself is a nonconducting fluid. Even though the amount of graphite needed to produce a conductive zone is small, there must be a connected film (Katsube and Mareschal, 1993) on regional scales. Intergranular graphite films are suggested to explain low resistivities in a 10 km deep borehole in Germany (Jodicke, 1992; Haak et al., 1991) and in the deep Precambrian shield of Canada (Katsube and Mareschal, 1993). Duba et al. (1994) emphasize that a suite of conductive accessory minerals (ilmenite, magnetite, pyrite, pyrrhotite) including graphite were measured in the German drill cores. A graphite explanation is not usually invoked in conductive rift settings because a continuous supply of deep fluids is expected. Also, there appears to be a strong correlation with temperature which is not expected for graphite. Graphite is often used as an explanation where a conducting zone doesn't have a corresponding seismic signature. This would be the consequence for thin graphite films but it is also expected for very low water fractions (~1 %). Such levels of connected water saturation result in orders of magnitude change in electrical conductivity but corresponding changes in seismic velocities are very small (Watanabe, 1993).

3E.5.3. Intergranular aqueous fluid-dihedral angle control

New experimental data (Holness, 1993) suggest that enhanced electrical conductivity of deep metamorphic rocks is caused by water-saturated, low-porosity continental crust which has profound rheological implications. These data concern the interconnectivity of intergranular (not fracture-controlled) fluids as a function of pressure and temperature in the ductile crustal environment. Results from Holness (1993) are simplified schematically in Figure 3E-16a where the concept of dihedral angle is also sketched (Fig. 3E-16b). The dihedral angle or wetting angle (Brenan, 1991) is the angle subtended by intersecting grain walls at pore corners in a re-

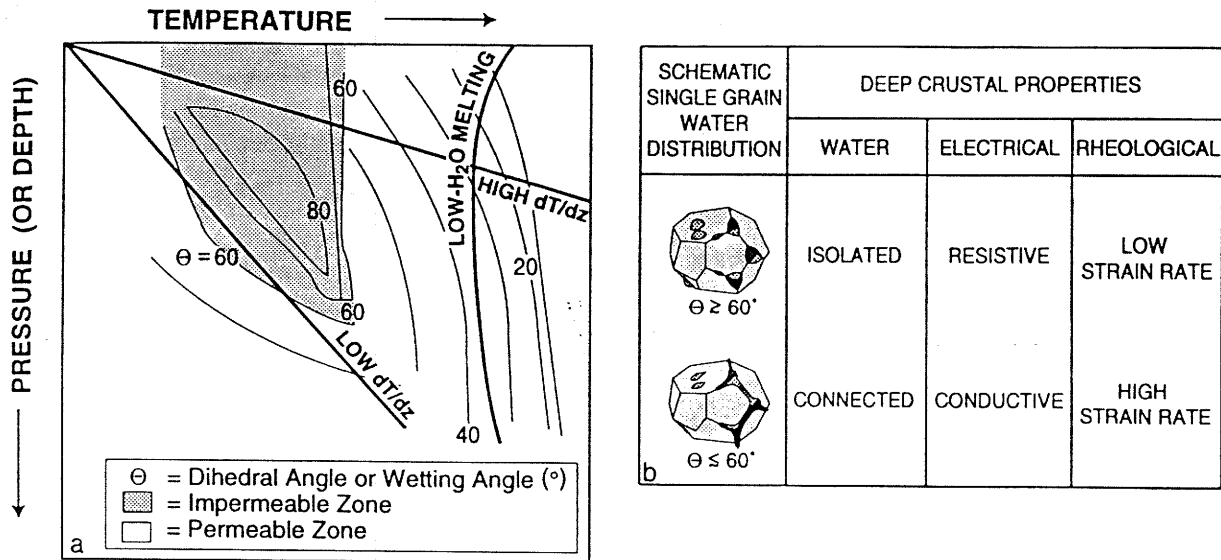


Fig. 3E-16. (a) Schematic pressure, temperature, dihedral angle plot for crustal conditions. Pattern of dihedral angle contours follows those of quartzite-H₂O system presented by Holness (1993). Shaded region is where aqueous fluids reside in isolated pores and the rock is impermeable to fluid flow ($\theta > 60^\circ$). At dihedral angles $\theta < 60^\circ$ the rock has an interconnected fluid phase and is permeable to grain-edge fluid flow. High and low dT/dz geothermal gradients illustrate situations where interconnected aqueous fluid would be trapped beneath an impermeable cap (shaded region). Notice that for various values of high dT/dz , the depth to the trapped fluid would vary but the temperature would be nearly constant following an isotherm. (b) Schematic single grain aqueous fluid distribution as a function of value of dihedral angle ($60^\circ < \theta < 60^\circ$); table of implications in deep crustal metamorphic rocks.

crystallized rock at equilibrium conditions. The values of dihedral angle define the 3-D continuity, therefore, interconnectivity of the grain-edge porosity. Interconnectivity can only exist if the angle is less than a critical value which is about 60° for 1% porosity (Hyndman, 1988). Total grain-edge wetting is achieved at 0° dihedral angle. Dihedral angle implications on crustal conductivity have been discussed (e.g., Hyndman, 1988; Marquis and Hyndman, 1992). However, the data were not adequate to define a pressure (depth)-temperature-dihedral angle plot as was done by Holness (1993). The published plot is for a pure quartzite-H₂O equilibrium system where the wet melting temperature is about 1100°C . Presumably this temperature would be near 640°C for a wet crust of granitic composition. Therefore, actual pressure and temperature values have been omitted in Figure 3E-16a since the

major features of a plot embracing the ductile portion of the crust are what we want to emphasize. Two hypothesized geothermal gradients are sketched in Figure 3E-16a. These illustrate that two regions of fluid connectivity may exist in the ductile crust under an impermeable cap ($\theta > 60^\circ$). For high geothermal gradients, fluid interconnectivity would occur at a near-constant temperature irrespective of the actual value of the geothermal gradient. The temperature is defined by the near-vertical contour of $\theta = 60^\circ$, which is almost parallel to the rock melting curve (Fig. 3E-16a). For lower geothermal gradients, the region of interconnectivity is at lower temperature nearer the brittle-ductile transition. The temperature at the top of the zone would vary considerably depending on the intersection of the geothermal gradient with the non vertical $\theta = 60^\circ$ contour. Note that if the geothermal gradient is very low, the

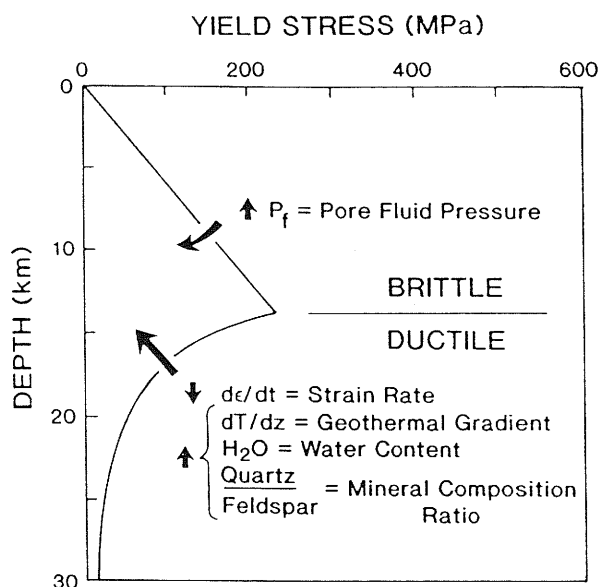


Fig. 3E-17. Synoptic diagram of crustal rheological behavior showing the effects of increasing pore fluid pressure in the brittle regime; and decreasing strain rate and increasing geothermal gradient, water content, and quartz/feldspar ratio in the ductile portion of the crust (redrawn from Sibson, 1984).

dihedral angle would be $<60^\circ$ throughout the entire region (depth range) plotted and there would be no impermeable cap. This would be the case of continuous dewatering of the crust even with a continuous source of deep aqueous fluid.

The dihedral angle considerations above present two situations where deep crustal conductive zones would have sharp upper boundaries. One, where the geothermal gradients are high, dictates that the depth to the conductive zone would be an isotherm. In the other case, at lower geothermal gradients, a deeper conductive zone would be at lower temperatures. More experimental results, such as those presented by Holness (1993) on actual rock/fluid assemblages expected throughout the crust, are needed to confirm or reject these expectations. Such a confirmation has just appeared (Holness, 1995) which presents results at 4 kbar pressure for the quartz- H_2O - CO_2 system with trace amounts of feldspar. Watson and Brenan (1987) reported on dihedral angle measurements performed principally on dunite and

quartzite with CO_2 - H_2O and solutes of NaCl and other salts. Their results are appropriate to conditions in the deep crust and upper mantle (950 – $1105^\circ C$ temperature and 1 GPa pressure) with a low percentage of aqueous brine solution. The major findings were that the effect of saline solutions was to decrease the dihedral angle to as low as 40° for the quartz-fluid system but there was no change in the high dihedral angle ($\theta \gg 60^\circ$) in dunite with, or without, salts. This implies that aqueous solutions are more likely to be interconnected in the ductile crust if the aqueous solution is saline but not so in the mafic mantle. The latter result agrees with a similar study reported on clinopyroxene-rich rocks (Watson and Lupulescu, 1993).

3E.5.4. Consequences of intergranular aqueous fluid

Watson and Brenan (1987) suggest that it is tempting to conclude that the dihedral angle-controlled fluid distributions apply to any conditions in the Earth where recrystallization has occurred, i.e., any pressure-temperature condition above the lowest metamorphic grade. In the case of a rift environment we must first ask whether or not the crust is in the required mechanical and chemical equilibrium. In fact, brittle fracturing occurs in active areas, such as rifts, even in the ductile regions of the crust as a result of tectonic stresses and igneous intrusions. These transient events deviate from static equilibrium but for rocks hot enough to undergo rapid plastic deformation, it is likely that equilibrium pore geometries develop rapidly (Brenan, 1991). For equilibrium wetting to occur, its rate must exceed the rate of ductile rock deformation; this is always the expected situation (Watson and Brenan, 1987).

It is clear from many experimental results (e.g., Kronenberg and Tullis, 1984; Cooper and Kohlstedt, 1986) that a connected fluid phase decreases the strength (the viscosity) of the rock and enhances the strain rate. The strength of the crust has the general profile depicted in Figure 3E-17 but there are several interdependent factors (Sibson, 1984) that can perturb it. In the ductile portion of the crust an increase in the geothermal gradient, water content, or quartz content will decrease the strength and the brittle-ductile transition will migrate upward. More

locally, a zone of interconnected water within the ductile region will facilitate increased pressure solution creep which enhances the strain rate. Experimentally, this effect is large where grain wetting occurs in olivine-basalt partial melts (Cooper and Kohlstedt, 1986). The process involves the diffusion of dissolved minerals along grain boundaries from regions of higher stress (at asperities) where the solubility is high to regions of low stress where the solubility is low (Turcotte and Schubert, 1982). This diffusion requires fluid interconnectivity.

Since an interconnected aqueous film has orders of magnitude higher conductivity compared to that of isolated pockets of H₂O, the connection with rheology as outlined above strongly suggests that the mapping of deep conductive zones is an indirect measurement of strain levels in the crust (Fig. 3E-15b). Thus, we made the assertion in our *Introduction* (§ 3E.1) that measurements of deep electrical resistivity may hold the key to understanding how continental rifts deform. The association of electrical resistivity with dihedral angle wetting is dependent on both pressure and temperature (Fig. 3E-16a) as well as rock type and fluid composition so the consequences are very far reaching. Therefore, we eagerly await more data relating the consequences of interconnected aqueous fluids in the crust with tectonic processes and geophysical properties, including electrical resistivity.

Acknowledgments. The most insightful discussions on the magnetotelluric method appear in notes that have never been published. Some of the best of these were done by U. Schmucker and P. Weidelt, F. Bostick, and the late G. Hohmann. The "theory section" of this contribution has benefited greatly from informally distributed Xerox copies of these works; in particular, one of us (GRJ) has subscribed to the approach learned at the University of California-Berkeley under the tutelage of S.H. Ward and H.F. Morrison and from fellow students including Jerry Hohmann. Much of this contribution comes from a condensation of notes used at San Diego State University and at the SAGE program (Summer of Applied Geophysical Experience). We thank more than 400 students who have critically reviewed the notes

and have led to continual changes and corrections. The writing of much of this was accomplished at the Los Alamos National Laboratory (LANL), Institute of Geophysics and Planetary Physics where GRJ was on sabbatical leave in 1994. The hospitality of the staff and director of the Institute, C.F. Keller, are warmly appreciated. Discussions with LANL petrologists W.S. Baldrige and D. Hickmott on the implications of dihedral angle wetting were very helpful. A careful critical review by P.E. Wannamaker is very much appreciated.

3E.6. References

- Bahr, K., 1988. Interpretation of the magnetotelluric impedance tensor: regional induction and local telluric distortion. *J. Geophys.*, 62: 119-127.
- Bailey, R.C., 1990. Trapping of aqueous fluids in the deep crust. *Geophys. Res. Lett.*, 17: 1129-1132.
- Banks, R.J. and Beamish, D., 1979. Melting in the crust and upper mantle beneath the Kenya Rift: evidence from Geomagnetic Deep Sounding experiments. *J. Geol. Soc. London*, 136: 225-233.
- Berdichevsky, M.N. and Dmitriev, V.J., 1976. Basic principles of interpretation of magnetotelluric sounding curves. In: A. Adam (Editor), *Geoelectric and Geothermal Studies*, KAPG Geophys. Monogr., Akademiai Kiado, Budapest, 164-22.
- Biehler, S., Ferguson, J., Baldrige, W.S., Jiracek, G.R., Aldern, J.L., Martinez, M., Fernandez, R., Romo, J., Gilpin, B., Braile, L.W., Hersey, D.R., Luyendyk, B.P. and C.L. Aiken, 1991. A geophysical model of the Española Basin, Rio Grande rift, New Mexico. *Geophysics*, 56: 340-353.
- Boehl, J.E., Bostick, F.X., Jr. and Smith, H.W., 1977. An application of the Hilbert transform to the magnetotelluric method: *Elec. Geophys. Res. Lab. Rept.*, Univ. Texas, Austin, 98 pp.
- Brenan, J., 1991. Development and maintenance of metamorphic permeability: implications for fluid transport. In: D. M. Kerrick (Editor), *Contact Metamorphism*. Mineral. Soc. Amer., *Reviews in Mineralogy*, 26: 291-319.
- Cagniard, L., 1953. Basic theory of the magnetotelluric method of geophysical prospecting. *Geophysics*, 18: 605-635.
- Chave, A.D. and Smith, J.T., 1994. On electric and magnetic galvanic distortion tensor decomposition. *J. Geophys. Res.*, 99: 4669-4682.
- Cooper, R.F. and Kohlstedt, D.L., 1986. Rheology and structure of olivine-basalt melts. *J. Geophys. Res.*, 91: 9315-9323.
- Dmitriev, V.I. and Berdichevsky, M.N., 1979. The fundamental model of magnetotelluric sounding: *Proc. IEEE*, 67: 1034-1044.
- Duba, A.L. and Shankland, T.J., 1982. Free carbon and electrical conductivity in the Earth's mantle. *Geophys. Res. Lett.*, 9: 1271-1274.

- Duba, A., Helkamp, S., Meurer, W., Nover, G. and Will, G., 1994. Evidence from borehole samples for the role of accessory minerals in lower-crustal conductivity. *Nature*, 367:59-61.
- Gamble, T.B., Goubau, W.M. and Clarke, J., 1979. Magnetotellurics with a remote reference. *Geophysics*, 44: 53-68.
- Garland, G.D., 1975. Correlation between electrical conductivity and other geophysical parameters. *Phys. Earth Planet. Interiors*, 10: 220-230.
- Gough, D.I., 1986. Seismic reflectors, conductivity, water and stress in the continental crust. *Nature*, 323: 143-144.
- Groom, R.W., and Bailey, R.C., 1989. Decomposition of magnetotelluric impedance tensor in the presence of local three-dimensional galvanic distortion. *J. Geophys. Res.*, 94: 1913-1925.
- Groom, R.W., and Bailey, R.C., 1991. Analytic investigations of the effects of near-surface three-dimensional galvanic scatterers on MT tensor decompositions. *Geophysics*, 56: 496-518.
- Groom, R.W. and Bahr, 1992. Corrections for near surface effects: Decomposition of the magnetotelluric impedance tensor and scaling corrections for regional resistivities: A tutorial. *Surv. Geophys.*, 13: 341-379.
- Haak, V. and Hutton, V.R.S., 1986. Electrical resistivity in continental lower crust. In: J.B. Dawson, D.A. Carswell, J. Hall and K.H. Wedepohl (Editors), *The Nature of the Lower Continental Crust*. Geol. Soc. London, Spec. Publ., 24: 35-49.
- Haak, V., Stoll, J. and Winter, H., 1991. Why is the electrical resistivity around the KTB hole so low?. *Phys. Earth Planet. Inter.*, 66: 12-23.
- Hermance, J.F., 1979. The electrical conductivity of materials containing partial melt: A simple model from Archie's law. *Geophys. Res. Lett.*, 6: 613-616.
- Hermance, J.F., 1982. Magnetotelluric and geomagnetic deep-sounding studies in rifts and adjacent areas: constraints on the physical processes in the crust and upper mantle. In: Special Volume on Continental and Oceanic Rifts, International Commission on Geodynamics. Am. Geophys. Union, Washington, DC, 8: pp. 169-192.
- Hermance, J.F. and Pedersen, J., 1980. Deep structure of the Rio Grande rift: A magnetotelluric interpretation. *J. Geophys. Res.*, 85: 3899-3912.
- Hobbs, B.A., 1992. Terminology and symbols for use in studies of electromagnetic induction in the earth. *Surv. Geophys.*, 13: 489-515.
- Holness, M. B., 1993. Temperature and pressure dependence of quartz-aqueous fluid dihedral angles: the control of adsorbed H₂O on the permeability of quartzites. *Earth Planet. Sci. Lett.*, 117: 363-377.
- Holness, M.B., 1995. The effect of feldspar on quartz-H₂O-CO₂ dihedral angles at 4 kbar, with consequences for the behavior of aqueous fluids in migmatites. *Contrib. Mineral. Petrol.*, 118: 356-364.
- Hyndman, R.D., 1988. Dipping seismic reflectors, electrically conductive zones, and trapped water in the crust over a subducting plate. *J. Geophys. Res.*, 93: 13,391-13,405.
- Hyndman, R.D. and Klemperer, S.L., 1989. Lower-crustal porosity from electrical measurements and inferences about composition from seismic velocities. *Geophys. Res. Lett.*, 16: 255-258.
- Hyndman, R.D. and Shearer, P.M., 1989. Water in the lower continental crust: modelling magnetotellurics and seismic reflection results. *Geophys. J. Int.*, 98: 343-365.
- Hyndman, R.D., Vanyan, L.L., Marquis, G. and Law, L.K., 1993. The origin of electrically conductive lower continental crust: saline water or graphite?. *Phys. Earth Planet. Inter.*, 81: 325-344.
- Jiracek, G.R., 1990. Near-surface and topographic distortions in electromagnetic induction. *Surv. Geophys.*, 11: 163-203.
- Jiracek, G.R., 1995. Geoelectromagnetics charges on. In: U.S. National Report to International Union of Geodesy and Geophysics, 1991-1994, Amer. Geophys. Union, in press.
- Jiracek, G.R., Ander, M.E. and Holcombe, H.T., 1979. Magnetotelluric soundings of crustal conductive zones in major continental rifts. In: Robert E. Riecker (Editor), *Rio Grande Rift: Tectonics and Magmatism*. Am. Geophys. Union, Washington DC, pp. 209-222.
- Jiracek, G.R., Gustafson, E. and Mitchell, P.S., 1983. Magnetotelluric results opposing magma origin of crustal conductors in the Rio Grande rift. *Tectonophysics*, 94: 299-326.
- Jiracek, G.R., Rodi, W.L. and Vanyan, L.L., 1987. Implications of magnetotelluric modeling for the deep crustal environment in the Rio Grande rift. *Phys. Earth Planet. Inter.*, 45: 179-192.
- Jodicke, H., 1992. Water and graphite in the earth's crust—an approach to interpretation of conductivity models. *Surv. Geophys.*, 13: 381-407.
- Jones, A.G., 1987. MT and reflection: an essential combination. *Geophys. J.R. Astron. Soc.*, 89: 7-18.
- Jones, A.G., 1992. Electrical conductivity of the continental lower crust, In: *The Continental Lower Crust*, edited by D.M. Fountain, R.J. Arculus, and R.W. Kay. Elsevier, New York, pp. 81-143.
- Katsube, T.J. and Mareschal, M., 1993. Petrophysical model of deep electrical conductors: graphite lining as a source and its disconnection due to uplift. *J. Geophys. Res.*, 98: 8019-8030.
- Kaufman, A.A., 1985. Tutorial: Distribution of alternating electrical charges in a conducting medium. *Geophys. Prosp.*, 33: 171-184.
- Keller, G.V., 1989. Electrical structure of the crust and upper mantle beneath the United States, Part 2, Survey of data and interpretation. In: L.C. Pakiser and W.D. Mooney (Editors), *Geophysical Framework of the Continental United States*, Geol. Surv. Amer. Mem. 172, Boulder, Colorado, 425-446.
- Kronenberg, A.K. and Tullis, J., 1984. Flow strengths of quartz aggregates: Grain size and pressure effects due to hydrolytic weakening. *J. Geophys. Res.*, 89: 4281-4297.
- Larsen, J.C., 1977. Removal of local surface conductivity effects from low frequency mantle response curves. *Acta Geod. Geophys. Mont.*, 12: 183-186.

- Madden, T. and Nelson, P., 1964. A defense of Cagniard's magnetotelluric method: Project NR-371-401. *Geophys. Lab., MIT*, 41 pp.
- Mareschal, M., Jouanne, V., Menvielle, M., Chouteau, M., Grandis, H. and Tarits, P., 1993. Magnetotelluric observations over the Rhine graben, France: A simple impedance tensor analysis helps constrain the dominant electric features. *Phys. Earth Planet. Inter.*
- Marquis, G. and Hyndman, R.D., 1992. Geophysical support for aqueous fluids in the deep crust: seismic and electrical relationships. *Geophys. J. Int.*, 110: 91-105.
- Merzer, A.M. and Klempner, S.L., 1992. High electrical conductivity in a model lower crust with unconnected, conductive, seismically reflective layers. *Geophys. J. Int.*, 108: 895-905.
- Newton, R.C., 1990. Fluids and shear zones in the deep crust. *Tectonophysics*, 182: 21-37.
- Olhoeft, G.R., 1981. Electrical properties of granite with implications for the lower crust. *J. Geophys. Res.*, 86: 931-936.
- Pedersen, J. and Hermance, J.F., 1978. Evidence for molten material at shallow to intermediate crustal levels beneath the Rio Grande rift at Santa Fe (abs.), *EOS Trans. AGU*, 59: 390.
- Reddy, I.K. and Rankin, D., 1974. Coherence functions for magnetotelluric analysis. *Geophysics*, 39: 312-320.
- Rokityansky, I.I., 1982. *Geoelectromagnetic Investigation of the Earth's Crust and Mantle*. Springer-Verlag, New York, 381 pp.
- Schmucker, U., 1964. Anomalies of geomagnetic variations in the southwestern United States. *J. Geomagn. Geoelectr.*, 15: 192-221.
- Schmucker, U., 1970. Analysis of geomagnetic variations in the southwestern United States. *Bull. Scripps Inst. Oceangr.*, 13: 165 pp.
- Schmucker, U. and Tezkan, B., 1988. 10 Jahre elektromagnetische Tiefenforschung im Rheingraben -eine Zusammenfassung mit Ausblick auf neuere Ergebnisse. In: V. Haak and J. Homilius (Editors), *Protokoll über das 12. Kolloquium "Elektromagnetische Tiefenforschung"*. Königstein im Taunus, 1-3 March, pp. 17-34.
- Sibson, R.H., 1984. Roughness at the base of the seismogenic zone: Contributing factors. *J. Geophys. Res.*, 89: 5791-5799.
- Sims, W.E. Bostick, F.X., Jr. and Smith, H.W., 1971. The estimation of magnetotelluric impedance tensor elements from measured data. *Geophysics*, 36: 938-942.
- Spies, B.R. and Eggers, D.E., 1986. The use and misuse of apparent resistivity in electromagnetic methods. *Geophysics*, 51: 1462-1471.
- Stenberg, B.K., Buller, P.L., Kisabeth, J.L. and Mehreteab, E., 1984. Electrical methods for hydrocarbon exploration: II. Magnetotelluric (MT) method. In: *Unconventional Methods in Exploration for Petroleum and Natural Gas*. S. Methodist Univ. Press., 220-230.
- Swift, C.M., Jr., 1967. *A Magnetotelluric Investigation of an Electrical Conductivity Anomaly in the Southwestern United States*. Ph.D. Thesis, Massachusetts Institute of Technology, Cambridge, Mass.
- Thompson, A.B. and Connolly, J.A.D., 1990. Metamorphic fluids and anomalous porosity in the lower crust. *Tectonophysics*, 182: 47-55.
- Tikhonov, A.N., 1950. Determination of the electrical characteristics of the deep strata of the earth's crust. *Dok. Akad. Nauk., USSR*, 73: 2, 295-297.
- Turcotte, D.L. and Schubert, G., 1982. *Geodynamics: Applications of Continuum Physics to Geological Problems*. John Wiley, New York, 450 pp.
- Vanyan, L.L., 1967. *Electromagnetic depth soundings*. Consultants Bureau, New York, 200 pp.
- Vozoff, K., 1972. The magnetotelluric method in the exploration of sedimentary basins. *Geophysics*, 37: 989-1014.
- Vozoff, K., 1991. The magnetotelluric method. In: Nabighian, M.N. (Editor), *Electromagnetic Methods in Applied Geophysics*, 2, B. Soc. Explor. Geophys., 641-711.
- Wait, J.R., 1954. On the relation between telluric currents and the earth's magnetic field. *Geophysics*, 19: 281-289.
- Wait, J.R., 1970. *Electromagnetic Waves in Stratified Media*. 2nd ed., Pergamon Press, New York.
- Wannamaker, P.E., Hohmann, G.W., and Ward, S.H., 1984. Magnetotelluric responses of three-dimensional bodies in layered earths. *Geophysics*, 49: 1517-1533.
- Ward, S.H. and Hohmann, G.W., 1988. Electromagnetic theory for geophysical applications. In: Nabighian, M.N., (Editor), *Electromagnetic Methods in Applied Geophysics—Theory*, 1. Soc. Explor. Geophys., 131-311.
- Watanabe, T., 1993. Effects of water and melt on seismic velocities and their application to characterization of seismic reflectors. *Geophys. Res. Lett.*, 20: 2933-2936.
- Watson, E.B. and Brenan, J.M., 1987. Fluids in the lithosphere, 1. Experimentally determined wetting characteristics of CO₂-H₂O fluids and their implications for fluid transport, host-rock physical properties and fluid inclusion formation. *Earth planet. Sci. Lett.*, 85: 497-515.
- Watson, E.B. and Lupulescu, A., 1993. Aqueous fluid connectivity and chemical transport in clinopyroxene-rich rocks. *Earth Planet. Sci. Lett.*, 117: 279-294.
- Wilson, M., 1989. *Igneous Petrogenesis*. Unwin Hyman, London, 466 pp.
- Zhang, P., Roberts, R.G. and Pederson, L.B., 1987. Magnetotelluric strike rules. *Geophysics*, 52: 267-278.
- Zhang, P., Pedersen, L.B., Mareschal, M. and Choteau, M., 1993. Channeling contribution to tipper vectors: A magnetic equivalent to electric distortion. *Geophys. J. Int.*, 113: 693-700.
- Zhdanov, M.S. and Keller, G., 1994. *The Geoelectrical Methods in Geophysical Prospecting*. Elsevier, Amsterdam, 900 pp.